Aus den
ViDia Christliche Kliniken Karlsruhe
Klinik für Hals-Nasen-Ohrenheilkunde
Kopf- und Halschirurgie und plastische Gesichtschirurgie

Diagnostic value of computed tomography of the temporal bone in Eustachian tube dysfunction

Inaugural-Dissertation
zur Erlangung des Doktorgrades
der Medizin

der Medizinischen Fakultät
der Eberhard Karls Universität
zu Tübingen

vorgelegt von

Kourtidis, Savvas

2020

Dekan: Professor Dr. B. Pichler

1. Berichterstatterin: Professorin Dr. med. S. Preyer
2. Berichterstatterin: Professorin Dr. med. U. Ernemann

Tag der Disputation: 06.10.2020

In dedication to the inspirational,
lovely and ever-smiling
Marie P.

Contents

List of Figures

List of Tables

List of graphs

Abbreviations

B	length of the bony part of Eustachian tube
B (test)	unstandardised regression coefficient
B1	length of the visualized bony part
B2	length of the non-visualized bony part
BETA	standardized regression coefficient
bp	bony portion
C	length of the cartilaginous part
C1	length of the visualized cartilaginous part
C2	length of the non-visualized cartilaginous part
Ca	curvature angle of Eustachian tube
COM	chronic otitis media
Cp	cartilaginous portion
CPR	curved planar reconstruction
CT	computed tomography
$CTDI_{vol}$	CT dose index
Df	degrees of freedom
Dif_	difference between normal and pathological side
ET	Eustachian tube
ETBD	balloon dilatation of the Eustachian tube
ETD	Eustachian tube dysfunction
ETDQ-7	Eustachian tube dysfunction questionnaire – 7
ETS-7	Eustachian tube score – 7
F	full length of Eustachian tube
F (test)	test F distribution
Fig	Figure
Graph	graphic
I	isthmus
Ia	inclination angle to Frankfurt horizontal plane
ICC	intra-class correlation coefficient
kV	kilovolt
L	most lateral of the Eustachian tube
M(point)	most medial of the Eustachian tube
M	mucus
MALT	mucosa-associated lymphoid tissue
mAs	milliampere-seconds
mm	millimeter
MPR	multiplanar reconstruction
MRI	magnetic resonance imaging
Norm_	normal sides measurements
NPV	negative predictive value
O	side of pathology
OME	Otitis Media with effusion
P	pharyngeal orifice
p	probability
Path_	pathological sides measurements
PPV	positive predictive value
R	correlation coefficient Pearson/ Spearman
R	radiologists' statement
R^2	R-squared
ROI	region of interest
S1	cross-sectional size of the pharyngeal orifice of Eustachian tube
S2	cross-sectional size of the tympanic orifice of Eustachian tube
SD	standard deviation
SNOT-22	sino-nasal outcome test – 22
t	paired sample t-test
T	tympanic orifice
Tab	Table
TMM	tubomanometry
UHR	ultra-high resolution
V1	visualization percentage of overall Eustachian tube lumen on Valsalva-CT-scan
V2	visualization percentage of cartilaginous lumen on Valsalva-CT-scan
V3	visualization percentage of bony lumen visualization on Valsalva-CT-scan
W	Shapiro Wilk test
Z	Wilcoxon Signed Rank test
3D	three dimensional

1. Introduction

1.1. Historical Background

The knowledge about the presence of the Eustachian tube reaches back to the ancient Egyptian times (1600 BC) [1]. First detailed anatomical characteristics of the Eustachian tube were obtained through anatomical dissections carried out by Bartolomeo Eustachio (1510-1574) [2,3], Antonio Maria Valsalva (1666 – 1723) [4,5] and Joseph Guichard Duverney (1648 – 1730) [6]. The role and functions of the Eustachian tube were first thoroughly described in physiology studies carried out by great otologists such as Adam Politzer (1835 – 1929) [7] and Joseph Toynbee (1815 – 1866) [8] during the second part of the 19th century. In recent times, a comprehensive understanding of the tubal function and its contribution to middle ear pathology was gained thanks to excellent pathophysiology studies (Bluestone CD, Poe D and Ars B) [9-12]. Modern advances in functional tests and non-invasive imaging modalities are promising to enlighten unknown aspects of tubal anatomy, physiology and pathophysiology in the following years.

1.2. Anatomy

The Eustachian tube, as part of serially connected organs including the palate, epipharynx, tympanic cavity, attic, aditus ad antrum, mastoid antrum and mastoid air cells, has a highly complex structure and localization [13] (Figure 1). Its anatomy is rather cleft-shaped than conduit-shaped [14], and it is located underneath the skull base [15]; it contains mucosa, cartilage and bone and is surrounded by soft tissue, such as the peri-tubal muscles (levator and tensor veli palatini, tensor tympani and salpingopharyngeus) and fat (Ostmann fat pad) [16]. It consists of two portions [15]:

1. A cartilaginous part, starting from the pharyngeal orifice (torus tubarius) and running posterior, lateral and superior to the sulcus tubae, between the temporal bone (petrous portion) and the sphenoid bone (greater wing) [15], and

2. An osseous part, starting from the overlapping or junction area (narrowest point – isthmus) and directing to the protympanic space of the middle ear cavity [15].

After birth, its' size constantly increases (approximately doubling) to reach 31-44 mm in adulthood [15,17,24]. The length ratio between the cartilaginous and the osseous part is approximately two thirds to one third, respectively. *"The angulation of the longitudinal axis of the Eustachian tube to the horizontal plane of the skull is approximately 30-40 degrees in adults"* [15,18]; in children the angle is much shallower angles (approximately 10 degrees) [18,19].

The lumen is covered by ciliated pseudostratified columnar epithelium (including mucosa-associated lymphoid tissue - MALT), which is essential for its function and is physiologically collapsed under normal ambient pressure conditions [14, 20]. The opening of Eustachian tube occurs briefly through (inter-)action of the peri-tubal muscles and is triggered passively via swallowing or movement of the mandible during chewing, speaking or yawning [10, 21-23].

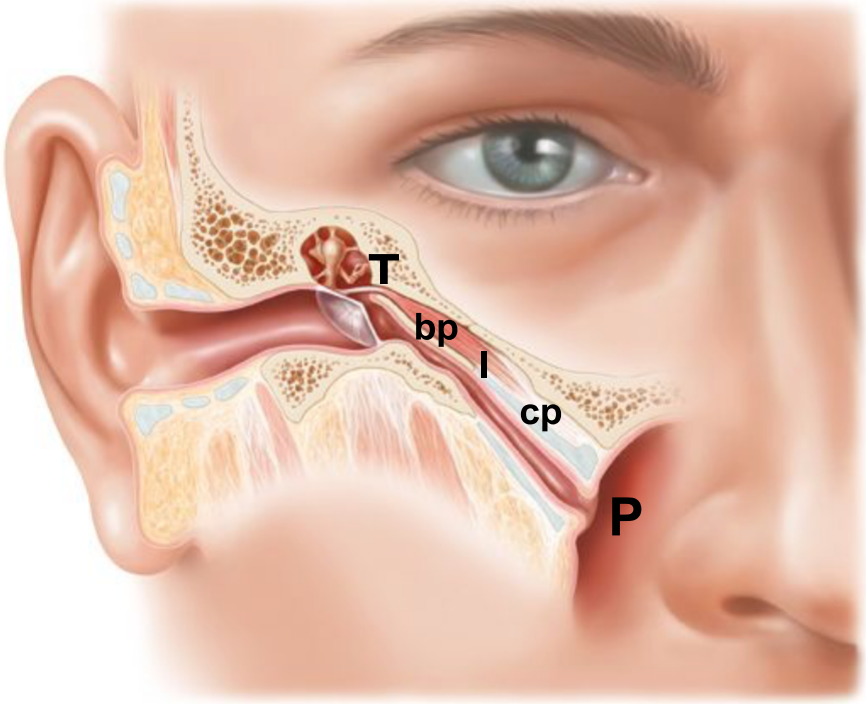

Figure 1. Localization and anatomy of the Eustachian tube. T: tympanic orifice, P: pharyngeal orifice, bp: bony portion, I: Isthmus, cp: cartilaginous portion (courtesy Spiggle & Theis Medizintechnik GmbH, Overath, Germany).

1.3. Physiology

The role of the Eustachian tube is thoroughly investigated and is crucial for the proper function of the middle ear, i.e. sound transmission from the tympanic membrane to the inner ear [9]. Nevertheless, unknown aspects are still present, due to the complexity and inaccessibility of the anatomic structures and their various interactions with extrinsic and intrinsic parameters. The main functions of the Eustachian tube are as follows [9]:

1. Ventilation of the *middle ear cavity* and *mastoid cell system* via ascending gas transfer from the nasopharynx.
2. Active and passive pressure equilibration of the middle ear cleft to the ambient atmospheric pressure.
3. Descending mucociliary clearance of secretions from middle ear cavity and mastoid cell system.
4. Mechanical protection against rhino-pharyngeal secretions from the nasopharynx and ascendant sound (vocals) during the speech.
6. Local immunological defence against ascendant infectious pathogens.

1.4. Pathophysiology - *Eustachian Tube Dysfunction*

According to the consensus statement of *"experts in the field of Eustachian tube disorders, Eustachian tube dysfunction (ETD) is defined, in its broader sense, as an impairment of one of the functions mentioned above"* [25]. In clinical practice, it comprises a failure of ventilatory and pressure equalization function. Therefore, it refers to a syndrome with a typical constellation of symptoms and signs resulting from pressure imbalance in the middle ear cavity: aural fullness and discomfort, subdued hearing, pressure in the ear, "popping" or "crackling", impaired equalization manoeuvre and autophony. "*The estimated prevalence in adults is approximately 1%; in children probably higher"* [26].
Three types of *Eustachian tube dysfunction* are distinguished according to the specialists' panel [25]:

1. *“Dilatory Eustachian tube dysfunction:*
    a. *Functional obstruction*
    b. *Dynamic obstruction*
    c. *Anatomical obstruction*
2. *Baro-challenge-induced Eustachian tube dysfunction*
3. *Patulous Eustachian tube dysfunction”*

Currently, there are neither international consented diagnostic criteria nor a “gold standard” investigation to diagnose these pathologic conditions and thus screening affected patients and measuring outcomes after therapeutic interventions poses a challenge for the physician [27]. A combination of patient history and symptoms, clinical signs (otomicroscopy, nasopharyngoscopy), audiometric tests (tubomanometry, tympanometry) and statistically validated questionnaires (*Eustachian tube score - 7* and *Eustachian tube dysfunction questionnaire - 7*, s. chapter 2.3 Materials and Methods) are used in daily clinical practice for the diagnosis of this condition and to measure treatment effect [28].

1.5. Radiologic diagnostics

High-resolution imaging studies provide an excellent method to evaluate the anatomical structure of the Eustachian tube. Furthermore, they are helpful in identifying accompanying pathologic conditions in the middle ear and nasopharynx, which could affect the proper function. Unfortunately, “no single modality provides details of all structures” [29]

- Computed tomography (CT) imaging is a widely available and economical imaging modality, which provides fast acquisition of high-resolution images; it is superior for osseous Eustachian tube, internal carotid canal and air-filled Eustachian tube lumen. It allows multiplanar reconstruction techniques and derivation of 3D images.
- Magnetic resonance imaging (MRI) imaging, in comparison, is superior for cartilaginous Eustachian tube and surrounding soft tissue elements. MRI

can provide detailed characteristics of the mucosa, cartilage, Ostmann fat pad and associated peri-tubal muscles.

Imaging investigations do not have an established role in assessing *Eustachian tube dysfunction* [25]. Therefore, Eustachian tube investigation remains a challenging task due to its' elaborate and tortuous anatomical course underneath the skull base and the collapsed, cleft-shaped lumen under resting conditions. The dynamic nature of Eustachian tube function in terms of middle ear aeration, mucociliary transport and fluid/sound protection makes this effort even harder. Several techniques, non-invasive or invasive, with or without contrast agents have been applied in experimental and clinical settings till to date; none of them could dominate in clinical practice as a single modality, appropriate to evaluate overall function [29].

1.6. Research aims

Since evidence regarding diagnostics of Eustachian tube function is currently sparse [27], the present study addresses the following objectives using clinical and radiological data elicited from current clinical practice with no extra cost, intervention or burden to the patient:

1. Determine whether morphological features of the Eustachian tube derived from CT-scans correlate with existent *Eustachian tube scores*, which reflect *Eustachian tube function*. Could radiological measurements be used as a valid diagnostic tool for *Eustachian tube dysfunction*?
2. Investigate whether the radiological detection of mucus in Eustachian tube or adjacent *middle ear cleft* structures is associated with *Eustachian tube dysfunction*. Is mucus a valid indicator to detect the side of pathology?
3. Determine whether secondary radiological findings regarding sinonasal pathology (i.e. chronic rhinosinusitis) are associated with *Eustachian tube scores*. Is the presence of occult chronic rhinosinusitis associated with *Eustachian tube dysfunction*?

4. Calculate the *sensitivity, specificity, positive and negative predictive value* of radiological evaluation on CT images to identify *Eustachian tube dysfunction*. Is the CT-scan an appropriate screening or diagnostic tool for *Eustachian tube dysfunction*?

2. Materials and Methods

2.1. Study Design

This trial is a mono-centric, prospective, cross-sectional case series trial. The clinical, as well as the radiological data collection, was conducted consecutively between June 2016 and June 2017 in the Otolaryngology Department of ViDia Christian Hospitals Karlsruhe, Germany. The radiological dataset was then blindly processed at the Diagnostic and Interventional Neuroradiology Department, University of Tuebingen, Germany. Finally, the statistical analysis was performed at the Institute for Clinical Epidemiology and Applied Biometry of the Medical Faculty of the University of Tuebingen, Germany. The local institutional review board of the Medical Faculty of the University of Tuebingen, Germany, approved this study. The study did not receive any third-party funding. Overall data were anonymized and treated consonantly with the principles of the latest version of the Declaration of Helsinki.

2.2. Patients

Eligible patients were 16 years and older with the diagnosis of unilateral *Eustachian tube dysfunction (ETD)*. The diagnosis was established through medical history, ear microscopy (± Valsalva manoeuvre), tympanometry, tubomanometry and use of the Eustachian Tube scores (*Eustachian tube score - 7* and *Eustachian tube dysfunction questionnaire - 7*, s. chapter 2.3.1.). Furthermore, the routine pre-therapeutic assessment included computed tomography of temporal bone while performing a Valsalva-manoeuvre (chapter 2.3.3.).

The study group comprised 80 Eustachian tubes of 40 patients (14 males aged mean 50,8 / SD 18,6 years and 26 females aged mean 49 / SD 16,7; age range 17-87). Twenty out of forty patients had an accompanying middle ear pathology, for example, recurrent seromucous otitis or retraction process of the tympanic membrane. All patients denied any pre-existing sinonasal disease.

2.3. Diagnostics

2.3.1. *Eustachian tube dysfunction questionnaire - 7 (ETDQ-7)*

The *"seven-item Eustachian tube dysfunction questionnaire or ETDQ-7"* (Table 1) is a statistically validated, easily administered, and robust patient-reported symptom score for identifying adult individuals suffering from *Eustachian tube dysfunction* [30]. It consists of seven disease-related questions, is side specific and has a quantitative response system ranging from *"1 (no problem) to 7 (severe problem)"* for each element. A total item score is consequently elicited, and the cutoff point is at 14,5, with an almost 100% sensitivity and specificity (discrimination between patients with ETD and healthy patients) [30,31]. Each patient filled the ETDQ-7 for each side as part of the routinely performed diagnostic assessment.

Table 1. *The seven-item Eustachian tube dysfunction questionnaire (ETDQ-7) [30]*

Over the past month, how much has each of the following been a problem for you?	*No problem*		*Moderate problem*			*Severe problem*	
1. Pressure in the ears?	*1*	*2*	*3*	*5*	*4*	*6*	*7*
2. Pain in the ears?	*1*	*2*	*3*	*4*	*5*	*6*	*7*
3. A feeling that your ears are clogged or "underwater"?	*1*	*2*	*3*	*4*	*5*	*6*	*7*
4. Ear symptoms when you have a cold or sinusitis?	*1*	*2*	*3*	*4*	*5*	*6*	*7*
5. Crackling or popping sounds in the ears?	*1*	*2*	*3*	*4*	*5*	*6*	*7*
6. Ringing in the ears?	*1*	*2*	*3*	*4*	*5*	*6*	*7*
7. A feeling that your hearing is muffled?	*1*	*2*	*3*	*4*	*5*	*6*	*7*

2.3.2. *Eustachian tube score - 7 (ETS-7*)

The *"Eustachian tube score seven or ETS-7"* (Table 2) is likewise a novel, easily applied and reliable instrument for screening individuals with *Eustachian tube dysfunction* [32]. It combines subjective patient estimations regarding the ability of perforiming Valsalva and Toynbee manoeuvre, objective ear microscopy findings during Valsalva manoeuvre, tympanometric and tubomanometric measurements (at 30, 40 and 50 mbar). In this way, a total item score for each Eustachian tube is derived, ranging from *"0 (pathologic condition) to 14 (healthy condition)"*. This test discriminates the pathologic condition with a sensitivity and specificity of 96%, at a cutoff point of 7 [32]. For each patient, the ETS-7 score was calculated for each side as part of the routinely performed diagnostic assessment.

Table 2. *The Eustachian tube score 7 (ETS-7). TMM = tubomanometry. [32]*

Symptom / finding	*2 points*	*1 point*	*0 points*
Clicking sound when swallowing	*always*	*occasionally*	*never*
Positive subjective Valsalva	*always*	*occasionally*	*never*
Objective Valsalva	*immediate*	*weak and slow*	*negative*
Tympanometry	*A*	*C*	*B*
TMM 30 mbar	*R ≤ 1*	*R > 1*	*no R*
TMM 40 mbar	*R ≤ 1*	*R > 1*	*no R*
TMM 50 mbar	*R ≤ 1*	*R > 1*	*no R*

2.3.3. Valsalva-CT-scan

All scans were acquired using a third-generation single-source CT (SOMATOM® Definition AS+, Siemens Healthcare, Erlangen, Germany) with a fully integrated circuit detector (Stellar® detector, Siemens Healthcare, Erlangen, Germany).

The imaging parameters were as follows: gantry rotation time, 1.0 second; tube current, 230 reference mAs using an automatic tube current modulation (CARE Dose4D®, Siemens Healthcare, Erlangen, Germany) yielding an average tube current of 201 mAs and an average CT dose index ($CTDI_{vol}$) of 41.3; tube voltage, 120 kV; and pitch, 0.85. The detector collimation was 16 × 0.3 mm using a z-axis UHR and flying focal spot technique [33], resulting in 0.4-mm slice thickness. The scans were reconstructed using ADMIRE (Siemens Healthcare, Erlangen, Germany) at a strength level of A2 [34].

During each CT scan of the temporal bone, the patient was instructed to simultaneously perform a Valsalva-maneuver to *"enhance the visualization of the lumen of the Eustachian tube"*, as previously described by Tarabichi et al. [35]. Detailed instructions were given by the technician to the patients how to perform a forceful exhalation against the closed nose (occlusion through digital compression). The patients were asked to maintain constant pressure during the whole duration of the scan. The CT-scan covered the skull base, including the entire anatomy of the Eustachian tube, the nasopharynx as well as the inner and middle ear structures. The image acquisition time was approximately 5 seconds.

2.4. Image analysis

2.4.1 Eustachian tube model

The S-shaped schematic model of Kikuchi et al. [36] was used to approximate the Eustachian tube anatomy and perform morphological analyses (Figure 2a-c). Previous studies showed that its shape is curved with significant interindividual variance, and its volume is age-dependent [24, 37-38]. "*Particularly in adults, the ET can be assumed as a gently curving, inverted S-shaped organ, although there is a range from almost straight to acutely curved [38]. Using CT with contrast injected into the ETs of cadavers, Oberascher et al. characterized the lumen shape like oval, except for the isthmus, which was found to be cylindrical [39]".*

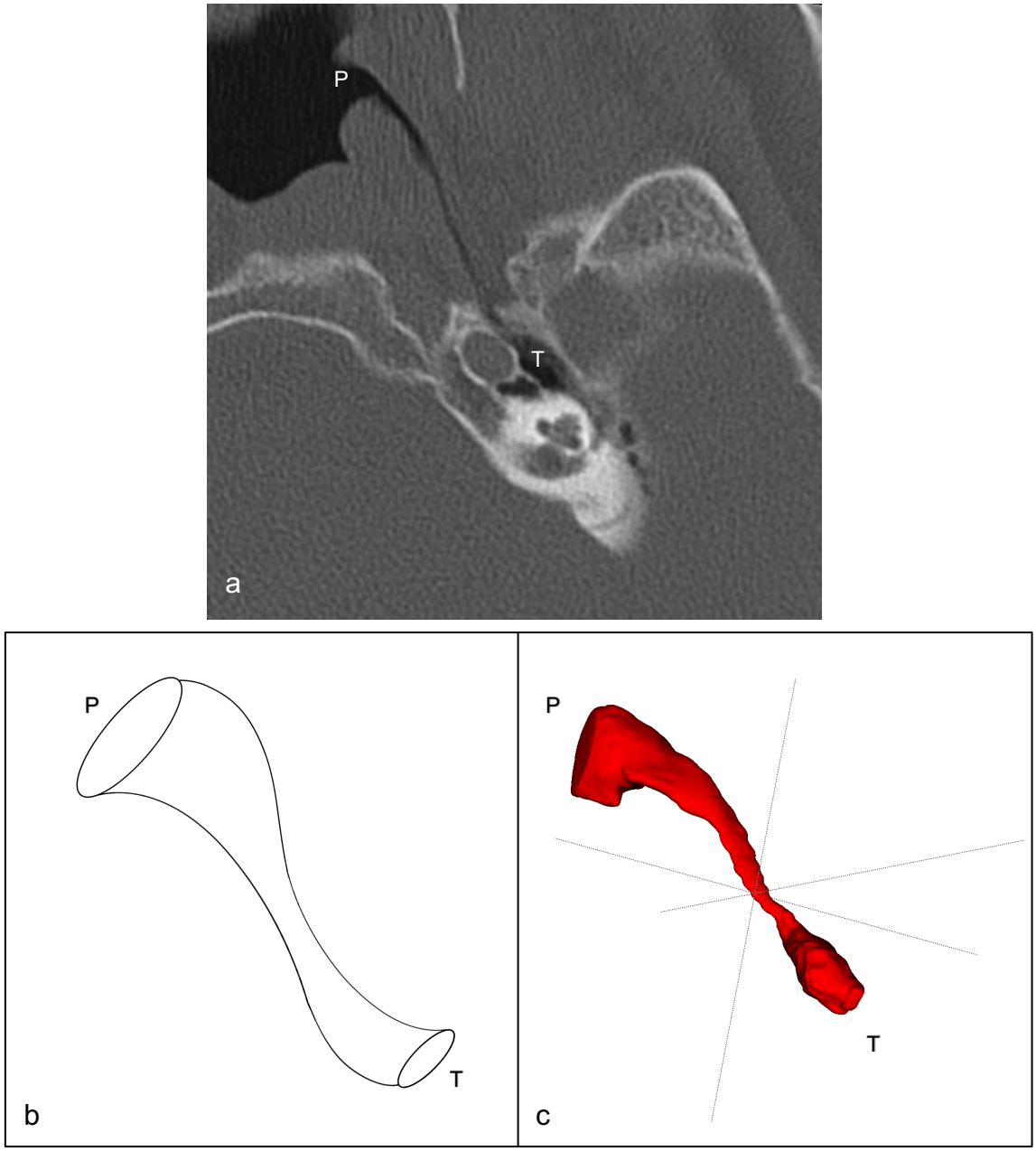

Figure 2 a. Complete visualization of Eustachian tube (ET) lumen traced as a transradiant line on oblique planes of Valsalva-CT-scan [own archive] b. ET model after Kikuchi et al. [36] [own archive] and c. 3D volume rendering using software application ITK-SNAP, www.itksnap.org [84], [own archive]. P: pharyngeal orifice, T: tympanic orifice.

2.4.2. Morphological measurements

Image analyses were performed independently by two board-certified neuroradiologists who were blinded to the clinical diagnoses. Before the study, both readers underwent a simulation training with a separate anonymized dataset, including ten temporal bone CT scans. Both readers had seven years of experience in temporal bone cross-sectional imaging. For inter-rater reproducibility, the intraclass correlation coefficient (ICC) was measured.

Image and region of interest (ROI) analyses were performed using Syngo.Via® (Siemens Healthcare, Erlangen, Germany). The Eustachian tube was delineated using a curved planar reconstruction (CPR). The following anatomical landmarks, according to Yoshida et al. [40,41] and Kikuchi et al. [36], were identified on the perpendicular images to the CPR centerline:

1. "The pharyngeal orifice of the Eustachian tube: the area nearest the nasopharynx where the Eustachian tube lumen appears semicircular."
2. "The tympanic orifice: the junction point in the delineated Eustachian tube between the posterior margin of the carotid canal and the basal turn of the cochlea" [modification due to different image reconstruction technique: in the present study curved planar reconstructions (CPR) versus axial multiplanar reconstruction (MPR) in Yoshida et al. [40,41] and Kikuchi et al. [36]]
3. "The isthmus: the junction point between the bony and soft tissue portion of the Eustachian tube."
4. "The cartilaginous part of the Eustachian tube: the segment from the pharyngeal orifice to the isthmus."
5. "The bony part of the Eustachian tube: the segment from the isthmus to the tympanic orifice."

Using these landmarks on the reconstructed CT images, the following parameters were measured:

S1: *Cross-sectional size of the pharyngeal orifice of Eustachian tube*

The measurement of the *cross-sectional size of the pharyngeal orifice* on the coronal plane (Figure 3).

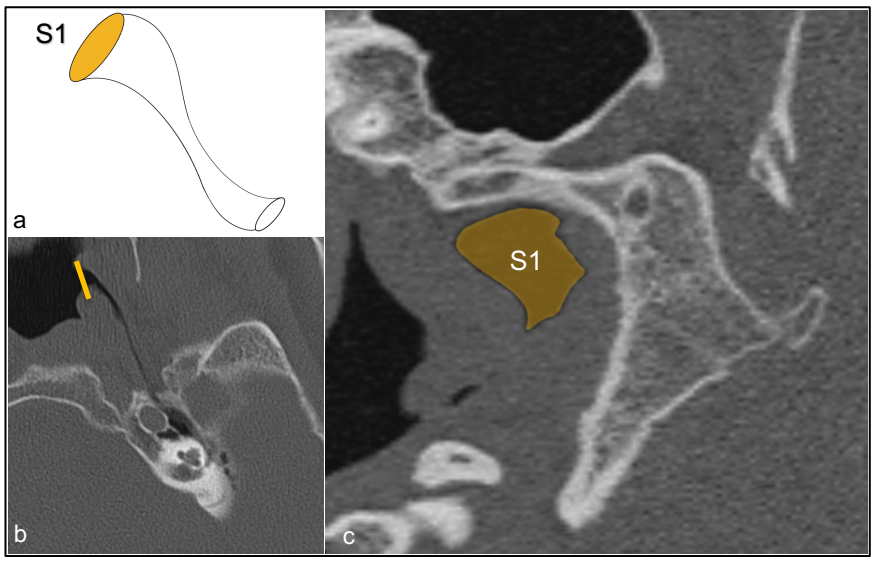

Figure 3. The *cross-sectional size of pharyngeal orifice* (S1) on a. ET model b. oblique plane and c. coronal plane [own archive].

S2: *Cross-sectional size of the tympanic orifice of Eustachian tube*

The measurement of the *cross-sectional size of the tympanic orifice* on the coronal plane (Figure 4).

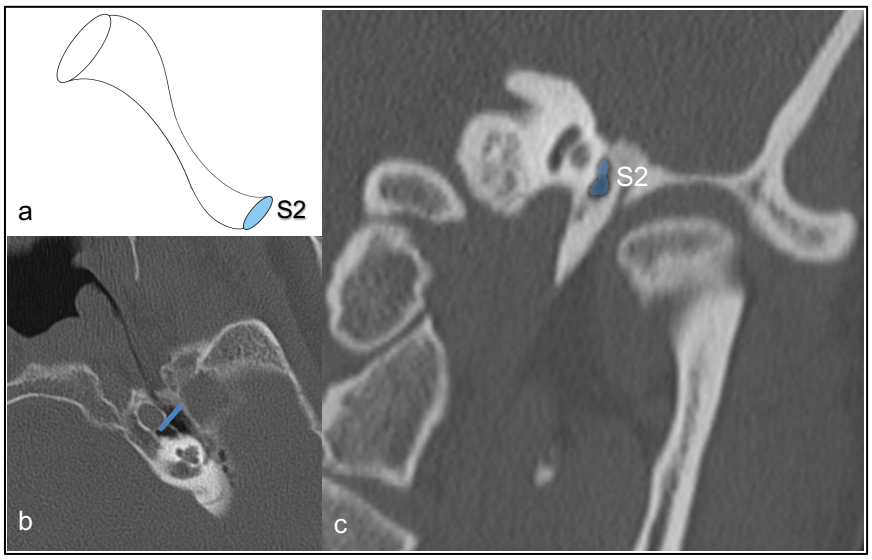

Figure 4. The *cross-sectional size of tympanic orifice* (S2) on a. ET model b. oblique plane and c. coronal plane [own archive].

F: *Full length of the Eustachian tube*

Tracing of the *Eustachian tube lumen* from the *pharyngeal* to the *tympanic orifice*, and measurement of its' full length on the oblique plane (Figure 5).

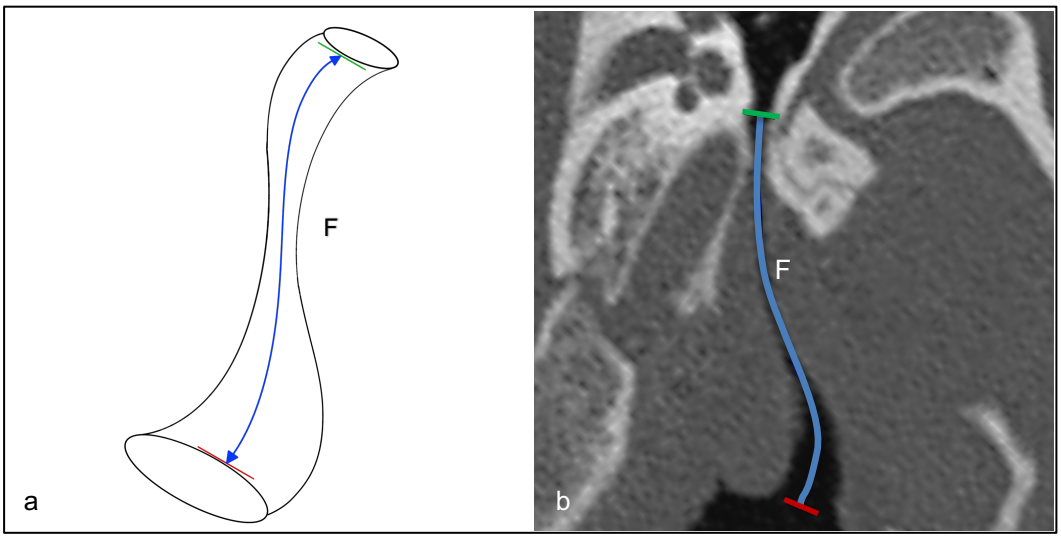

Figure 5. *Full length of Eustachian tube* (F) on a. ET model and b. oblique plane [own archive].

C: Length of cartilaginous part, **C1**: Length of visualized cartilaginous part, **C2**: length of the non-visualized cartilaginous part

The lumen of the cartilaginous Eustachian tube was traced as a hyper-lucent stripe starting from the *pharyngeal orifice* and directing to the isthmus. The full length of the cartilaginous portion was measured, as well as the visualized and non-visualized (collapsed) parts of it on oblique planes (Figure 6).

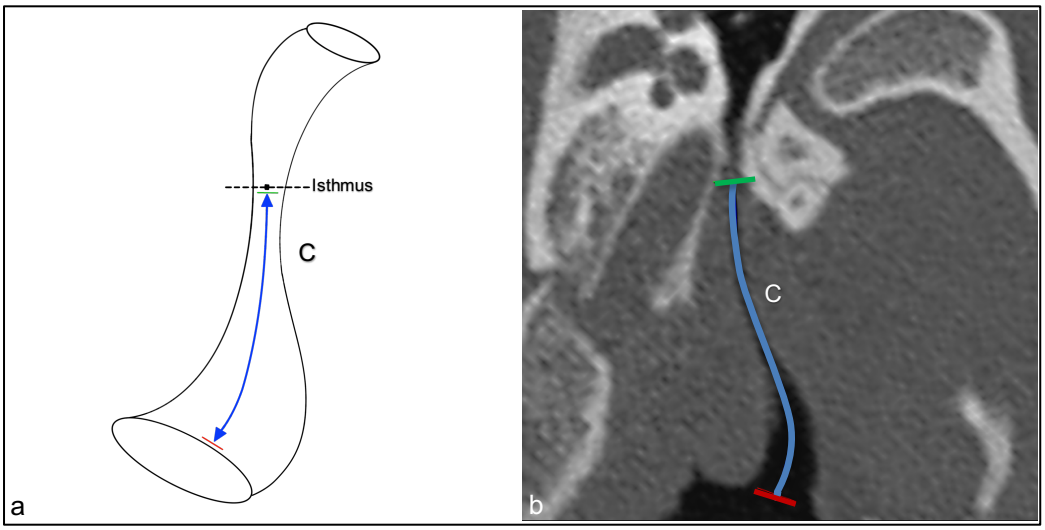

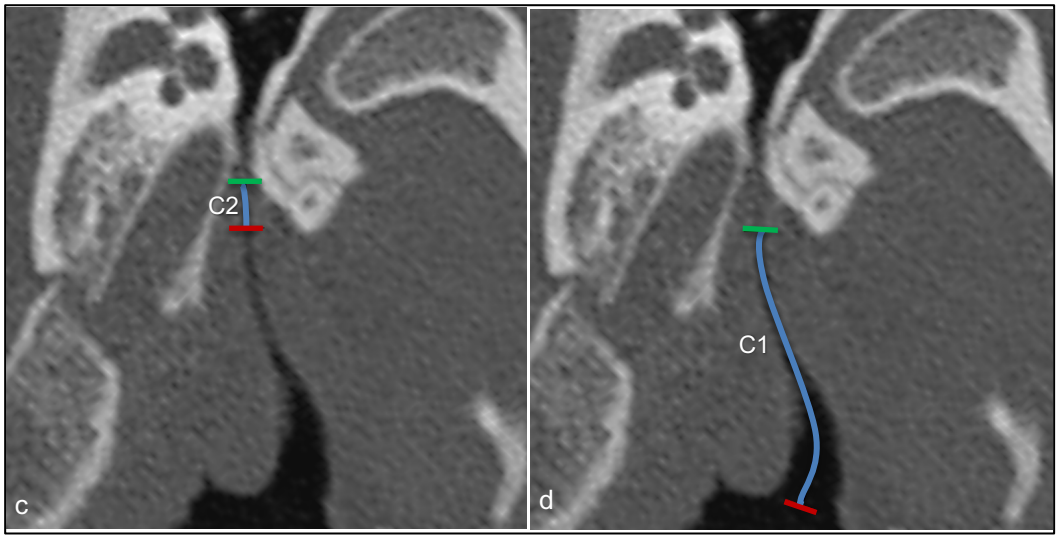

Figure 6. Full length of the cartilaginous portion of the Eustachian tube (C) on a. ET model and b. oblique planes., c. non-visualized cartilaginous part (C2) and d. visualized cartilaginous part (C1) [own archive].

B: length of the bony part of Eustachian tube, **B1**: length of the visualized bony part, **B2**: length of the non-visualized bony part

The lumen of the bony Eustachian tube was traced as a hyper-lucent stripe starting from the isthmus and directing to the *tympanic orifice*. The full length of the bony portion was measured, as well as the visualized and non-visualized parts of it (Figure 7).

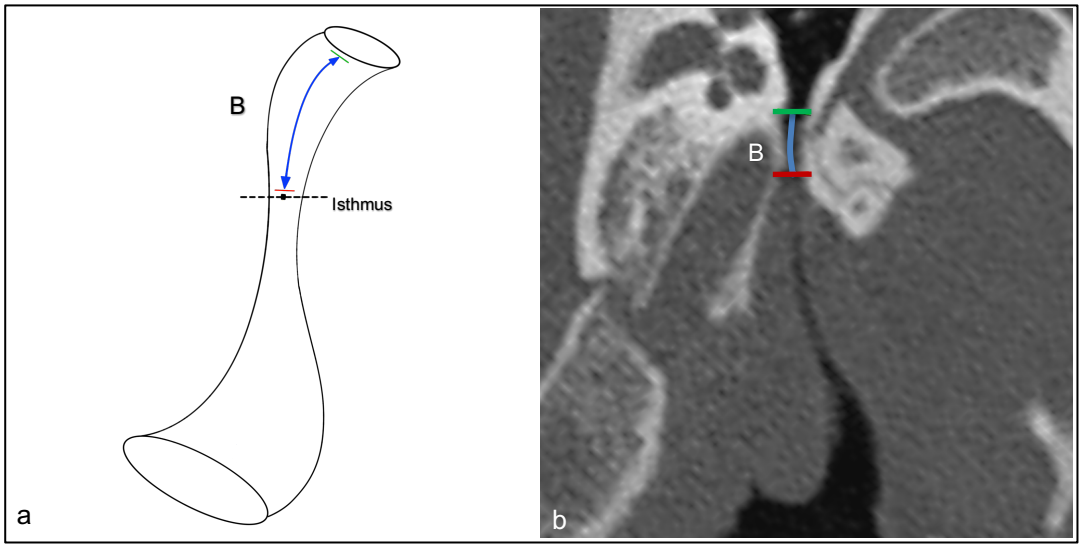

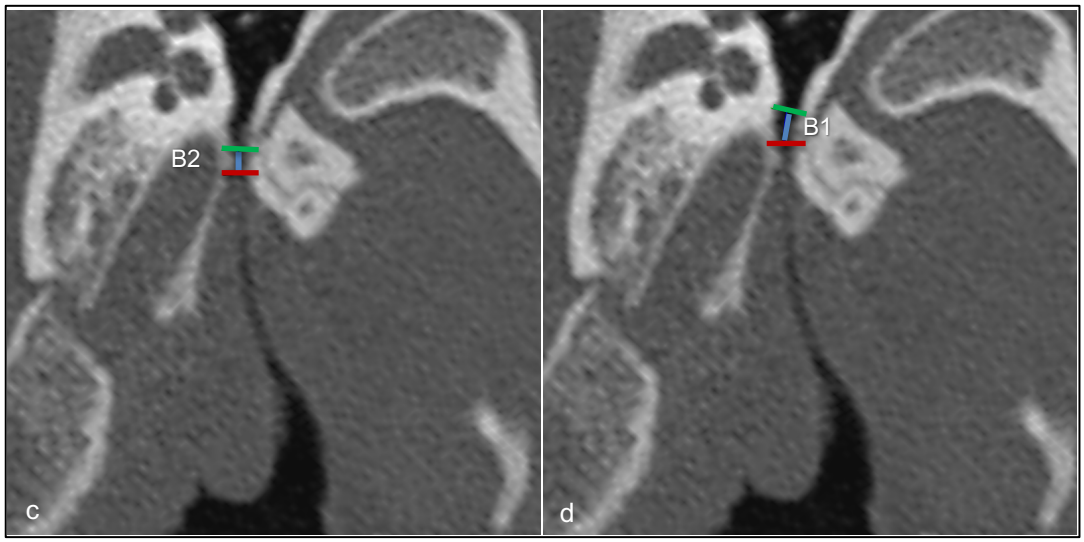

Figure 7. Full length of the bony portion of the Eustachian tube (B) on a. ET model and b. oblique planes. c. non-visualized bony part (B2) and d. visualized bony part (B1) [own archive].

I: *Inclination angle to Frankfort horizontal plane*

Delineation of the inclination angle (Ia) on the sagittal MPR between Frankfort horizontal plane [42] and the *tympanic orifice* (T) (Figure 8).

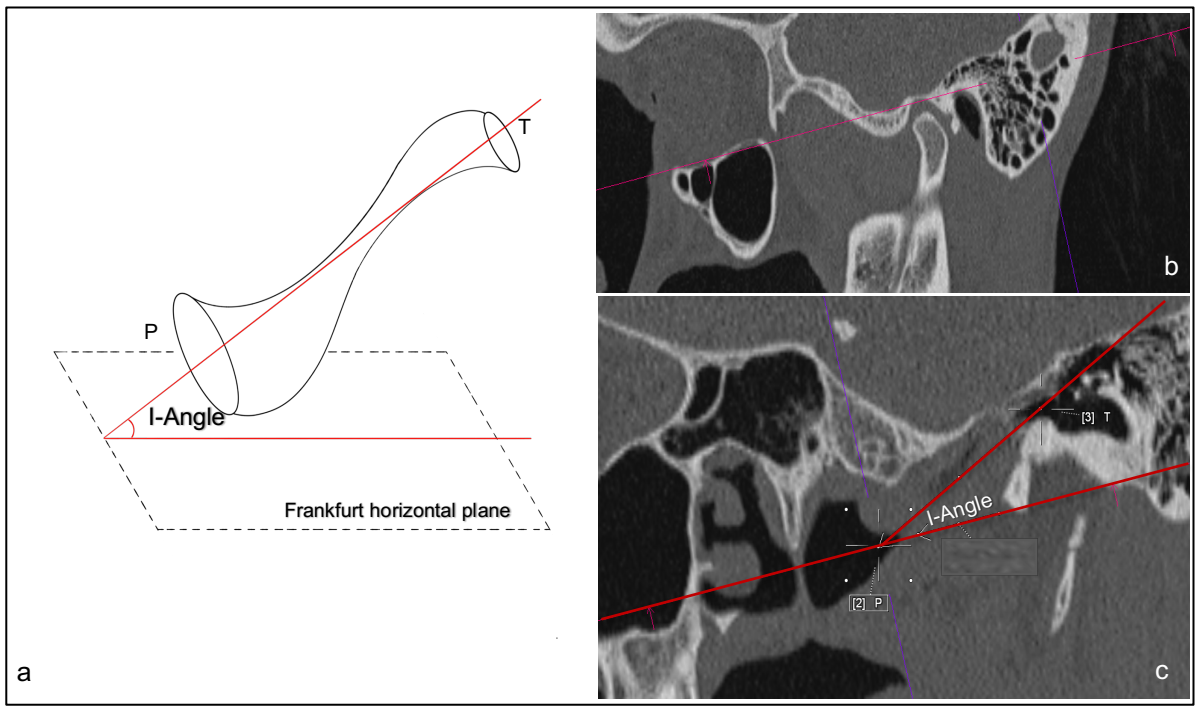

Figure 8. Inclination angle (Ia) of the Eustachian tube (B) on a. ET model and b. coronal and c. oblique planes [own archive]. P: *pharyngeal orifice*, T: *tympanic orifice*.

Points **P**, **T**, **L** and **M**

"The 3D coordinates for the centre of the pharyngeal (P) and the tympanic (T) orifice as well as for the most medial (M) and most lateral (L) points of the Eustachian tube lumen were identified" [36] (Figure 9). These 3D coordinates were used to calculate the curvature angle (Ca) of the Eustachian tube and thus characterizing its S-shape (larger C angle → deeper curvature, smaller C-angle → swallower curvature).

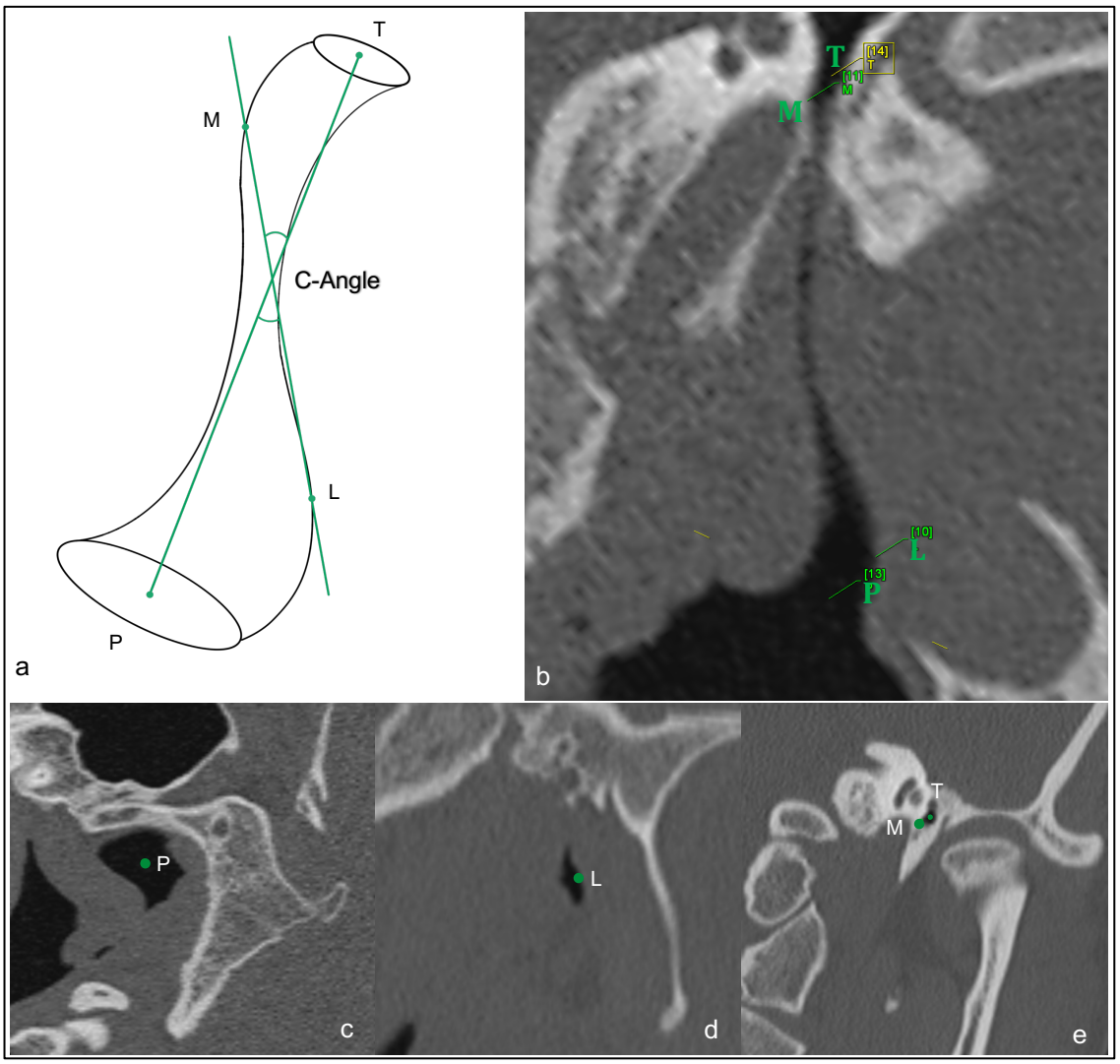

Figure 9. Curvature angle (Ca) of the Eustachian tube on a. ET model, b. P, L, T, M points on oblique planes, c., d., e., P, L, T, M points on coronal planes [own archive].

After performing these measurements, seven morphological parameters were derived to conduct correlation studies with the Eustachian tube scores:

1. **S1***: the cross-sectional size of the pharyngeal orifice of Eustachian tube*
2. **S2**: *the cross-sectional size of the tympanic orifice of Eustachian tube*
3. **V1**: visualization percentage of overall Eustachian tube lumen on Valsalva-CT-scan: derived from F, B, B1, B2, C, C1 and C2
4. **V2**: visualization percentage of cartilaginous lumen on Valsalva-CT-scan: derived from C, C1 and C2
5. **V3**: visualization percentage of bony lumen visualization on Valsalva-CT-scan: derived from B, B1 and B2
6. **Ia**: inclination angle to Frankfort horizontal plane
7. **Ca**: curvature angle of the S-shaped Eustachian Tube (derived from 3D coordinates of the P, T, L and M points)

2.4.3. Subjective image analysis – radiologists' statement

All CT images were reviewed for visual pathology of the bony middle ear structures as well as the adjacent nasopharynx and the nasal sinuses. Particular focus was laid on obstruction of the tympanic or pharyngeal orifice by mucus or fluid retention or other signs of chronic tympanic or mastoid ventilation disorder. Finally, a statement was derived: the radiologists (always blinded to the side of pathology) determined whether a Eustachian tube is pathologic or normal according to their personal clinical experience in reviewing CT-scans of the temporal bone, without taking into account the morphologic measurements previously described (2.3.2. Morphologic measurements). The average duration of image post-processing, delineation of the ET, the definition of the anatomical landmarks, and qualitative image analysis was 15 minutes for one side.

2.5. Statistical analysis

Statistical analysis was performed at the Institute for Clinical Epidemiology and Applied Biometry, Medical Faculty of University of Tübingen, Germany). The software used for this purpose was IBM SPSS Statistics (IBM Corp. Released 2016. IBM SPSS Statistics for Windows, Version 24.0. Armonk, NY: IBM Corp.). Descriptive as well as inferential statistical methods were used; a p-value <0.05 was considered to signalize statistical significance. In detail:

For the 1st research aim, descriptive statistics (frequencies/percentages for categorical variables and mean/standard deviation/medians for continuous variables) were utilized to summarize the cohort's characteristics. Intraclass correlation coefficients (ICC) were calculated to prove the reproducibility of morphologic measurement outcomes over different examiners. The Shapiro-Wilk test and the histogram parameters of skewness and kurtosis analyzed the Gaussian distribution in the clinical and the radiological variables. Following, non-parametric Wilcoxon rank test and parametric t-test compared the mean and median values between the pathological and healthy sides. The Pearson and Spearman correlation coefficients identified correlations between morphological features and results of the clinical *Eustachian tube scores*. Finally, multivariate regression models were constructed for significant cases from univariate analysis.

For the 2nd research aim, the paired (dependent) sample t-test was used to test the presence of mucus in pathological and normal sides. Thereby the association between mucus and *Eustachian tube dysfunction* was measured.

For the 3rd research aim, the non-parametric McNemar test for nominal variables was used to investigate the association of accompanying nose pathology with the pathological side. Also, independent samples t-test has been performed to check if the presence of an accompanying ear pathology or accompanying sinonasal pathology or combinations of them (either, both) are affecting the *Eustachian tube scores ETDQ – 7* and *ETS-7*.

For the 4th research aim, the *sensitivity, specificity, positive predictive value (PPV) and negative predictive value (NPV)* were calculated to investigate the validity of the subjective radiological assessment of patients with *Eustachian tube dysfunction*.

3. Results

3.1. Cohort characteristics

The baseline characteristics of the study group are summarized in Table 3.

Table 3. Baseline characteristics of the study group

Demographic characteristics	All patients (n=40)	
Age mean	50	
Age range	17 - 87	
Age Standard Deviation	17,2	
Age median	51	
Gender	14 males / 26 females	
Percentage (%)	35% males / 65% females	
Pathologic conditions		
Side of pathology	22 left side / 18 right side	
Percentage (%)	55 % / 45%	
Accompanying ear pathology	20 with accompanying ear pathology / 20 without	
Percentage (%)	50% / 50 %	
Eustachian tube scores		
ETDQ-7	mean	standard deviation
Normal side	10,7	4,8
Pathologic side	25,4	9,9
ETS7		
Normal side	10,2	2,8
Pathologic side	5,2	3

3.2. Statistical analysis

3.2.1. 1st research aim

Are morphological measurements of Eustachian tube correlating with the Eustachian tube scoring system? Could radiological measurements be used as a valid diagnostic tool for *Eustachian tube dysfunction*?

Summary of Eustachian tube scores and morphological measurements

The variables, i.e. the Eustachian tube scores and the morphological measurements, are summarized below:

ETDQ-7: clinical *Eustachian tube score*
ETS-7: clinical *Eustachian tube score*
S1: *the cross-sectional size of the pharyngeal orifice of Eustachian tube*
S2: *the cross-sectional size of the tympanic orifice of Eustachian tube*
V1: visualization percentage of overall Eustachian tube lumen on Valsalva-CT-scan
V2: visualization percentage of cartilaginous lumen on Valsalva-CT-scan
V3: visualization percentage of bony lumen on Valsalva-CT-scan
Ia: inclination angle to Frankfort horizontal plane
Ca: curvature angle of the S-shaped Eustachian Tube

Test for inter-rater reliability

The morphological characteristics of Eustachian tubes were measured independently by two board-certified neuroradiologists, who were blinded to the clinical diagnoses. For inter-rater agreement, the Intraclass Correlation Coefficient [ICC: two-way mixed-effects model, absolute agreement, average measures] and their 95% confident intervals were calculated (Table 4).

Table 4. Results of the Intraclass Correlation Coefficient.

	ICC	95% Confidence Interval		F Test	p
		Lower Bound	Upper Bound	value	value
Average measures	.991	.989	.993	114,4	.000

The average measure ICC was .991 with a 95% confidence interval from .989 to .993 (F(212)=114,484, p=.000<.001).

Tests for data distribution

a. Normal sides measurements (Norm_ = values of healthy sides).

Table 5 represents results of normality tests using Shapiro Wilk and Skewness/Kurtosis for the variables Norm_ETDQ7, Norm_ETS7, Norm_S1, Norm_S2, Norm_V1, Norm_V2, Norm_V3, Norm_Ca and Norm_Ia.

Shapiro Wilk: null hypothesis is that variables are normally distributed and the alternative that they are not. Variable Norm_S1 is normally distributed (W(40)=0,979, p=0,646>0,05) as well as variables Norm_V1 (W(40)=0,960, p=0,169>0,05), Norm_V3 (W(40)=0,958, p=0,140>0,05) and Norm_Ia (W(40)=0,972, p=0,413>0,05). Variable Norm_ETDQ7 is not normally distributed (W(40)=0,777, p=0,000<0,05) as well as Norm_ETS7 (W(40)=0,927, p=0,013<0,05), Norm_S2 (W(40)=0,895, p=0,001<0,05), Norm_V2 (W(40)=0,916, p=0,006<0,05) and Norm_Ca (W(40)=0,933, p=0,021<0,05).

Skewness/Kurtosis: values of skewness and kurtosis between -1 and 1 were found in normally distributed variables, confirming the results of the Shapiro Wilk test performed previously. A mismatch to Shapiro Wilk test was observed in variable Norm_ETS7 (Skewness = -,605 and Kurtosis = -,469). After looking to the corresponding histogram, we assumed Norm_ETS7 as not normally distributed.

Table 5. Distribution of Norm_values.

Variables	Skewness	Kurtosis	W	df	p-value
Norm_ETDQ7	1,693	3,677	,777	40	,000
Norm_ETS7	-,605	-,469	,927	40	,013
Norm_S1	,472	,242	,979	40	,646
Norm_S2	1,376	2,742	,895	40	,001
Norm_V1	-,234	-,967	,960	40	,169
Norm_V2	-,378	-1,038	,916	40	,006
Norm_V3	-,483	-,127	,958	40	,140
Norm_Ca	1,032	2,880	,933	40	,021
Norm_Ia	,071	-,461	,972	40	,413

b. Pathological sides measurements (Path_ = values of pathological sides).

Table 6 indicates results of normality tests using Shapiro Wilk and Skewness/Kurtosis for variables Path_ETDQ7, Path_ETS7, Path_S1, Path_ S2, Path_V1, Path_V2, Path_V3, Path_Ca and Path_Ia.

Shapiro Wilk: null hypothesis is that variables are normally distributed and the alternative that they are not. Variable Path_ETDQ7 is normally distributed (W(40)=0,971, p=0,380>0,05) as well as variables Path_ ETS7 (W(40)=0,974, p=0,485>0,05), Path_S1 (W(40)=0,974, p=0,479>0,05), Path_S2 (W(40)=0,971, p=0,380>0,05) and Path_Ca (W(40)=0,985, p=0,856>0,05). Variable Path_V1 is not normally distributed (W(40)=0,917, p=0,006<0,05) as well as Path_V2 (W(40)=0,899, p=0,002<0,05), Path_V3 (W(40)=0,774, p=0,000<0,05) and Path_Ia (W(40)=0,943, p=0,043<0,05).

Skewness/Kurtosis: values of skewness and kurtosis between -1 and 1 were found in normally distributed variables, confirming the results of the previously performed Shapiro Wilk test. A marginal mismatch was found in two variables (Path_V1: Kurtosis = -,996, Path_Ia: Kurtosis = -,881). This mismatch may be due to their tendency to have values close to the cutoff-point of -1. However, after

looking at the corresponding histograms, they were considered as not normally distributed.

Table 6. Distribution of Path_ values.

Variables	Skewness	Kurtosis	W	df	p-value
Path_ETDQ7	,300	-,735	,971	40	,380
Path_ETS7	,240	-,474	,974	40	,485
Path_S1	,462	-,067	,974	40	,479
Path_S2	,345	-,432	,971	40	,380
Path_V1	-,544	-,996	,917	40	,006
Path_V2	-,314	-1,370	,899	40	,002
Path_V3	-1,551	1,478	,774	40	,000
Path_Ca	,394	,007	,985	40	,856
Path_Ia	,282	-,811	,943	40	,043

c. *Difference between the normal and pathological side (Dif_ = value of normal side – value of pathological side).*

Table 7 indicates results of normality tests using Shapiro Wilk and Skewness/Kurtosis for the variables Dif_ETDQ7, Dif_ETS7, Dif_S1, Dif_S2, Dif_V1, Dif_V2, Dif_V3, Dif_Ca and Dif_Ia.

Shapiro Wilk: null hypothesis is that variables are normally distributed and the alternative that they are not. Variable Dif_ETDQ7 is normally distributed (W(40)=0,97, p=0,357>0,05) as well as variables Dif_ETS7 (W(40)=0,962, p=0,197>0,05), Dif_S1 (W(40)=0,98, p=0,687>0,05), Dif_V1 (W(40)=0,964, p=0,234>0,05) and Dif_Ia (W(40)=0,977, p=0,590>0,05). Variable Dif_S2 is not normally distributed (W(40)=0,937, p=0,027<0,05) as well as Dif_V2 (W(40)=0,797, p=0,000<0,05), Dif_V3 (W(40)=0,840, p=0,000<0,05) and Dif_Ca (W(40)=0,886, p=0,001<0,05).

Skewness/Kurtosis: values of skewness and kurtosis between -1 and 1 were found in normally distributed variables, confirming the results of the Shapiro Wilk test performed previously.

Table 8 summarizes the distribution of test results.

Table 7. Distribution of Dif_ values.

Variables	Skewness	Kurtosis	W	df	p-value
Dif_ETDQ7	-,437	-,151	,970	40	,357
Dif_ETS7	-,529	-,158	,962	40	,197
Dif_S1	,034	-,706	,980	40	,687
Dif_S2	,985	2,254	,937	40	**,027**
Dif_V1	,633	,356	,964	40	,234
Dif_V2	1,982	6,595	,797	40	**,000**
Dif_V3	1,513	1,879	,840	40	**,000**
Dif_Ca	1,411	5,631	,886	40	**,001**
Dif_Ia	,189	-,500	,977	40	,590

Table 8. Summary of data distribution results.

Variable	Distribution	Variable	Distribution	Variable	Distribution
Norm_ETDQ7	not normal	Path_ETDQ7	normal	Dif_ETDQ7	normal
Norm_ETS7	not normal	Path_ETS7	normal	Dif_ETS7	normal
Norm_S1	normal	Path_S1	normal	Dif_S1	normal
Norm_S2	not normal	Path_S2	normal	Dif_S2	not normal
Norm_V1	normal	Path_V1	not normal	Dif_V1	normal
Norm_V2	not normal	Path_V2	not normal	Dif_V2	not normal
Norm_V3	normal	Path_V3	not normal	Dif_V3	not normal
Norm_Ca	not normal	Path_Ca	normal	Dif_Ca	not normal
Norm_Ia	normal	Path_Ia	not normal	Dif_Ia	normal

Mean and Median Comparison Analysis

Non-parametric paired samples Wilcoxon Signed Rank Test compared medians of values between the pathological and healthy side, because of the non-normal distribution of data either in one or the other group (except variable S1, see Table 8). Furthermore, the parametric paired sample T-test was performed due to its' "robustness" to violations of normality, to cross-check the outcomes and compare the mean values in both groups.

Null hypotheses are that the median of differences between the healthy and pathological sides equals zero and the mean values of morphological measurements between healthy and pathological sides are equal respectively. Table 9 summarizes coinciding results. A statistically significant difference of medians and means of variables V1 (Z = -2,124, p = 0,034 < 0,05 and t(39) = 2,427, p = 0,020 < 0,05 respectively) and V3 (Z = -2,177, p = 0,029 < 0,05 and t(39) = 2,817, p = 0,008 < 0,05 respectively) between the healthy and pathological sides could be found.

Table 9. Medians and Means comparison between normal and pathologic sides.

Morphological measurements	**N**	**Healthy side**	**Pathological side**	**Wilcoxon Signed Rank test**	**Paired Sample T-Test**
		mean (SD)	Mean (SD)	Z (p-value)]	t (p-value)
S1 (m^2)	40	34.7 (16,1)	31,2 (14,1)	-1,529 (,126)	1,670 (,103)
S2 (m^2)	40	12,5 (5,3)	11,2 (4,4)	-1,378 (,168)	1,534 (,133)
V1 (%)	**40**	**72,4 (17,4)**	**66,9 (24,1)**	**-2,124 (,034)**	**2,427 (,020)**
V2 (%)	40	67,9 (27)	66,2 (29,5)	-,143 (,886)	,628 (,533)

V3 (%)	**40**	**80,7 (12,1)**	**67,91 (28,9)**	**-2,177 (,029)**	**2,817 (,008)**
Ca (º)	40	10,4 (3,3)	9,6 (3,3)	-1,183 (,237)	1,254 (,217)
Ia (º)	40	30,1 (3,9)	29,8 (3,6)	-,316 (,752)	,461 (,647)

Correlation analysis

Two separate correlation analyses were performed: primary for Dif_ values, i.e. difference between the normal and pathological side and secondary for Path_ values, i.e. absolute values of the pathological side.

a. Correlation analysis for Dif_ variables

- *Dif_ETDQ7*

Non-parametric coefficient Spearman was used to correlate Dif_ETDQ7 with the non-normally distributed variables Dif_S2, Dif_V2, and Dif_V3, Dif_Ca, whereas parametric Pearson coefficient analyzed correlations between Gaussian distributed variables Dif_ETDQ7, Dif_S1, Dif_V1, and Dif_. Spearman's and Pearson's coefficients take values in the interval [-1,1].

Values close to 1 indicate strong positive correlation while values close to -1 strong negative. Values close to 0 indicate no correlation. The null hypothesis is that variables are correlated and the alternative that they are not. Table 10 indicates that variable Dif_ETDQ7 does not correlate with any other variable.

Table 10. Correlation analysis for Dif_ETDQ7.

Correlations	Dif_ETDQ7	Coefficient
Dif_S1	0,225	Pearson
Dif_S2	0,065	Spearman
Dif_V1	0,030	Pearson
Dif_V2	0,173	Spearman
Dif_V3	-0,028	Spearman
Dif_Ca	-0,013	Spearman
Dif_Ia	0,138	Pearson

- *Dif_ETS7*

Non-parametric coefficient Spearman was used to identify correlations between Dif_ETS7 and the non-normally distributed variables Dif_S2, Dif_V2, Dif_V3, and Dif_Ca. Pearson coefficient correlated the values of normally distributed variables Dif_ETS7, Dif_S1, Dif_V1, and Dif_Ia. Table 11 and graphs 1 & 2 indicate that variable Dif_ETS7 is positive correlated with variables Dif_V1 (r=0,462, p<0,01, Pearson) and Dif_V3 (r=0,598, p<0,01, Spearman).

Table 11. Correlation analysis for Dif_ETS7.

Correlations	Dif_ETS7	Coefficient
Dif_S1	-0,194	Pearson
Dif_S2	0,032	Spearman
Dif_V1	**,436****	Pearson
Dif_V2	0,020	Spearman
Dif_V3	**,598****	Spearman
Dif_Ca	-0,152	Spearman
Dif_Ia	-0,094	Pearson

**. Correlation is significant at the 0.01 level (2-tailed).

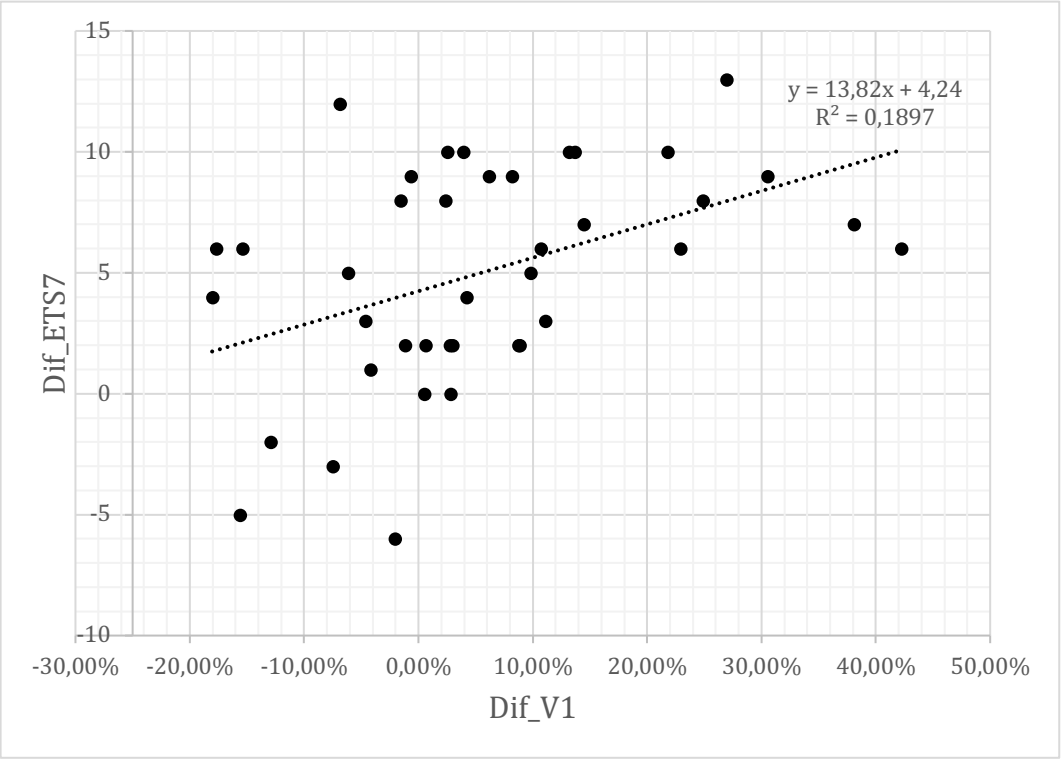

Graph 1. Scatter diagram Dif_ETS7 * Dif_V1.

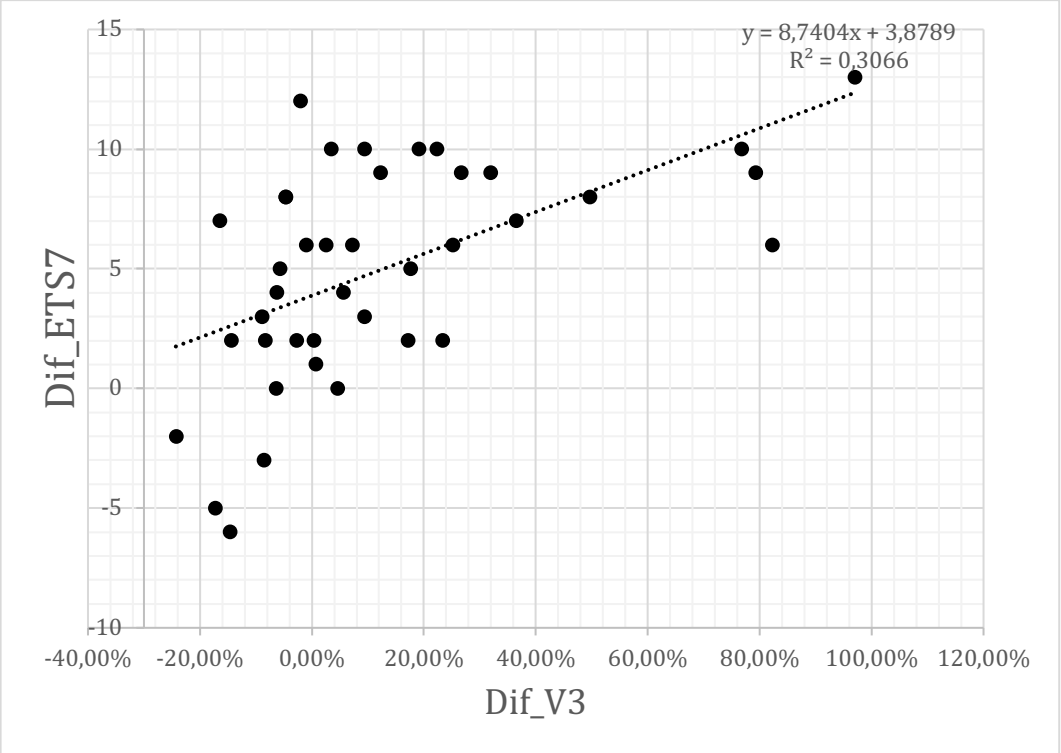

Graph 2. Scatter diagram Dif_ETS7*Dif_V3.

b. Correlation analysis for Path_ variables

- Path_ETDQ7

Non-parametric coefficient Spearman was used to identify correlations between variable Path_ETDQ7 and variables Path_V1, Path_V2, Path_V3 and Path_Ia, which are not normally distributed. Parametric coefficient Pearson was used to identify correlations between variable Path_ETDQ7 and variables Path_S1, Path_S2 and Path_Ca, which are normally distributed. Table 12 indicates that variable Path_ETDQ7 is not correlated with any variable.

Table 12. Correlation analysis for Path_ETDQ7.

Correlations	Path_ETDQ7	Coefficient
Path_S1	-0,014	Pearson
Path_S2	0,050	Pearson
Path_V1	0,090	Spearman
Path_V2	0,127	Spearman
Path_V3	-0,052	Spearman
Path_Ca	0,163	Pearson
Path_Ia	-0,066	Spearman

- Path_ETS7

Non-parametric coefficient Spearman was used to identify correlations between variable Path_ETS7 and variables Path_V1, Path_V2, Path_V3 and Path_Ia, which are not normally distributed. Parametric coefficient Pearson was used to identify correlations between variable Path_ETS7 and variables Path_S1, Path_S2 and Path_Ca, which are normally distributed. Table 13 and graphs 3 & 4 indicate that variable Path_ETS7 is correlated with variables Path_S2 ($r=0,361$, $p<0,05$, Pearson) and Path_V1 ($r=0,382$, $p<0,05$, Spearman).

Table 13. Correlation analysis for Path_ETS7.

Correlations	Path_ETS7	Coefficient
Path_S1	,102	Pearson
Path_S2	**,361***	Pearson
Path_V1	**,382***	Spearman
Path_V2	,289	Spearman
Path_V3	,290	Spearman
Path_Ca	,004	Pearson
Path_Ia	,170	Spearman

*. Correlation is significant at the 0.05 level (2-tailed).

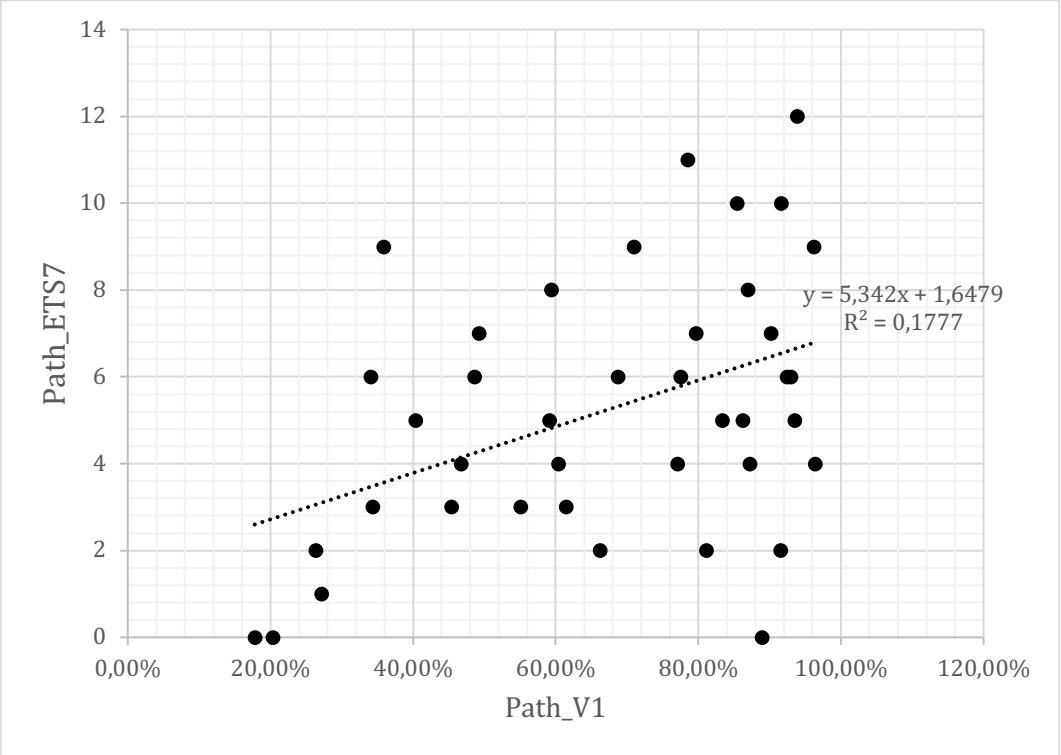

Graph 3. Scatter diagram Path_ETS7 * Path_V1.

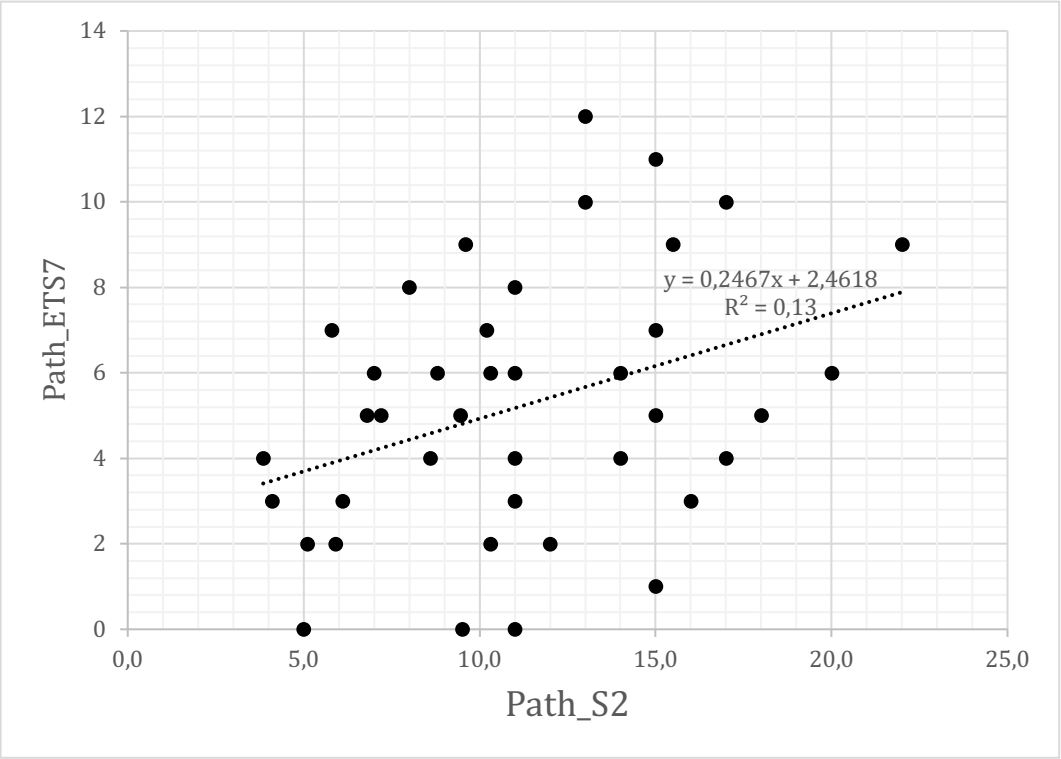

Graph 4. Scatter diagram Path_ETS7 * Path_S2.

Regression analysis

a. Regression analysis for Dif_ETS7

Multivariate regression model further investigated significant cases from the univariate correlation analysis. The aim was to establish a prediction model. Several linear regression variable selection methods (for example, forward selection, backward elimination) determined the best-fitting model. Table 14 indicates the results of the linear regression model fit using as dependent variable Dif_ETS7 and independent variables Dif_V3 and Dif_Ca. Null hypothesis, that model does not fit data, is rejected (F(2,37)=13,14, p=0,000<0,05). Level of adjustment was good as Adjusted $R^2 = 0,384 \cong 0,4$.

Table 14. Results of the linear regression model fit for Dif_ETS7.

R	R^2	Adj R^2	F	df1	df2	p-value
,644*	,415	,384	13,14	2	37	,000

* Predictors: (Constant), Dif_V3, Dif_Ca

Table 15 indicates that statistically significant indicators for dependent variable Dif_ETS7 are Constant (p=0,000<0,05) as well as variables Dif_V3 (p=0,000<0,05) and Dif_Ca (p=0,013<0,05). Dif_ETS7 could be predicted using the following mathematical formula:

Dif_ETS7= 4,08 + 0,09 x Dif_V3 – 0,39 x Dif_Ca

Table 15. Coefficients of multiple linear regression model for Dif_ETS7.

Independent variables	B	BETA	p-value
(Constant)	4,084		,000
Dif_V3	0,092	,586	,000
Dif_Ca	-,398	-,331	,013

Dependent variable: Dif_ETS7

The influence (Graph 5) of variable Dif_V3 (BETA=0,586) is greater of Dif_Ca (BETA=-0,331). Lastly, the graph 6 represented the results of Dif_ETS7 and estimated Dif_ETS7 by the multiple linear models.

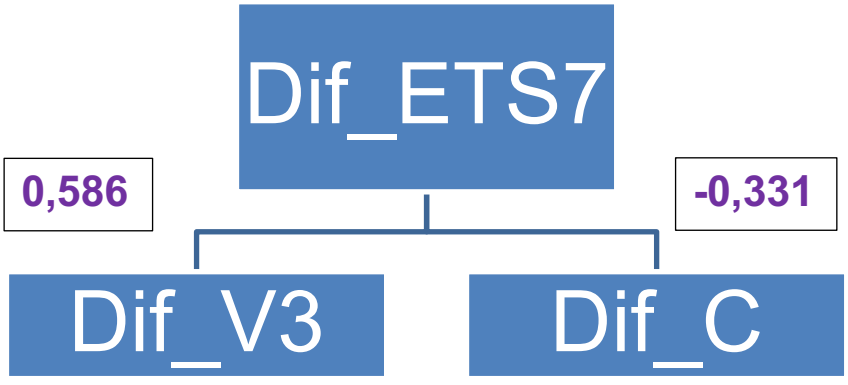

Graph 5. Influence of independent variables to Dif_ETS7.

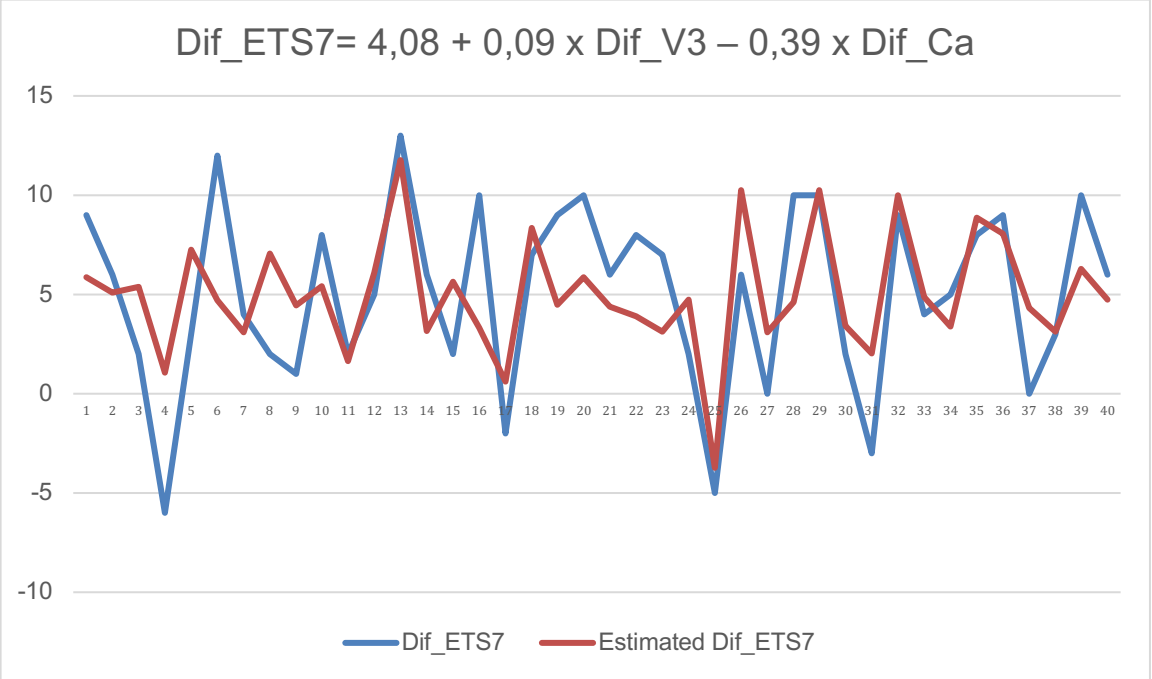

Graph 6. Prediction Model for Dif_ETS7.

b. Regression analysis for Path_ETS7

Table 16 indicates the results of the linear regression model fit using as dependent variable Path_ETS7 and independent variables Path_V3 and Path_S2. Null hypothesis, that model does not fit data, is rejected (F(2,37)=7,195, p=0,002<0,05). Level of adjustment was moderate as Adjusted R^2 = 0,241 < 0,4.

Table 16. Results of the linear regression model fit for Path_ETS7.

R	R^2	Adj R^2	F	df1	df2	p-value
,529*	,280	,241	7,195	2	37	,002

* Predictors: (Constant), Path_V3, Path_S2

Table 17 indicates that statistically significant indicators for dependent variable Path_ETS7 are variables Path_V3 (p=0,008<0,05) and Path_S2 (p=0,048<0,05). Path_ETS7 can be predicted using the following mathematical formula:

Path_ETS7= 0,16 + 0,04 * Path_V3 + 0,2 * Path_ S2

Table 17. Coefficients of multiple linear regression model for Path_ETS7.

Independent variables	B	BETA	p-value
(Constant)	,167		,907
Path_V3	,042	,393	,009
Path_S2	,200	,292	,046

Dependent variable: Path_ETS7

Influence (graph 7) of variable Path_V3 (BETA=0,393) is greater of Path_S2 (BETA=0,292). Graph 8 represents differences between Path_ETS7 and estimated Path_ETS7 by the multiple linear models.

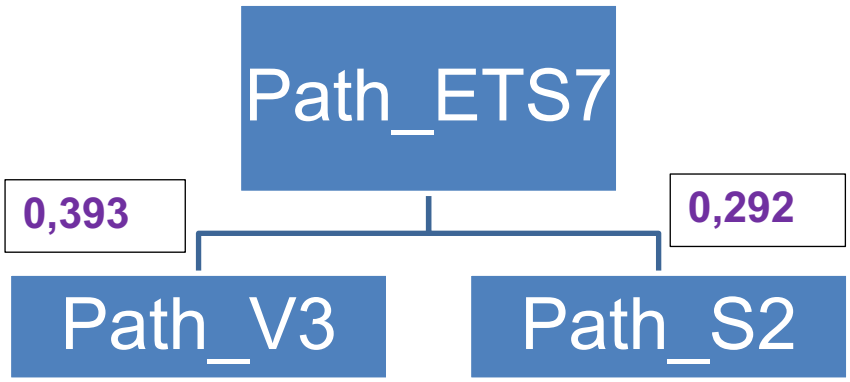

Graph 7. Influence of independent variables to Path_ETS7.

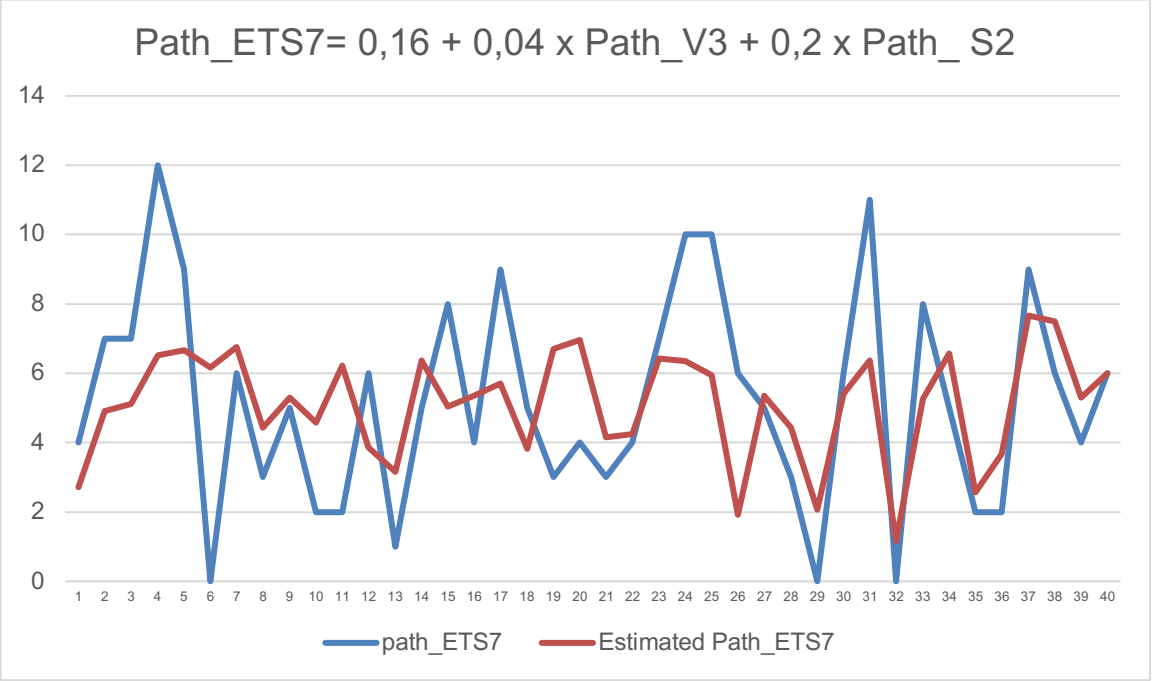

Graph 8. Prediction Model for Path_ETS7.

3.2.2. 2nd research aim

Is the radiological presence of mucus (M) in Eustachian tube or adjacent middle ear cleft structures associated with the pathological side? Is mucus a valid indicator to detect the side of pathology?

Table 18 summarizes the results of mucus detection in normal and pathological sides. Mucus only occurred on pathological sides (n=10/40; 25%).

Nevertheless, parametric paired sample t-test for dichotomic variables “pathological side” and “normal side” (no mucus versus mucus) was performed by common consent (no other statistical test could fit better in this case). The null hypothesis is that mean values are equal and the alternative that they are not. Table 18 indicates that mean value of mucus presence in pathological side (M=25%) is statistically significant greater (t(39)=3,606, p=0,001<0,05) than mean value of mucus presence in normal side (M=0%). Graph 9 represents the results.

Table 18. Mucus presence in the pathological and healthy side.

Side	Mucus (M)	Mean	N	df	t	p-value
pathological	10	25%	40	39	3,606	**0,001**
normal	0	0%	40			

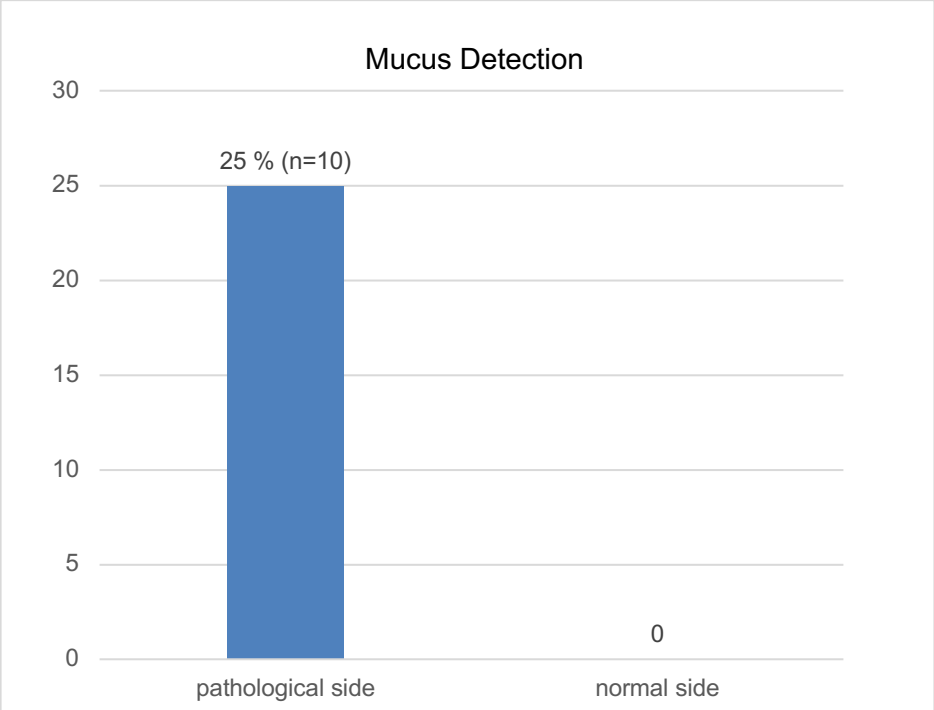

Graph 9. Mucus presence in pathological and healthy sides.

3.2.3. 3rd research aim

Is the radiological detection of accompanying sinonasal pathology associated with the pathological side? Is the presence of accompanying sinonasal pathology or combination of accompanying nose and ear pathology affecting ETDQ-7 and ETS-7 scores?

A 2x2 contingency Table for the normal and the pathological side displays the outcomes 0 = no detection of accompanying sinonasal pathology and 1 =

detection of accompanying sinonasal pathology (Table 19). The null hypothesis is that marginal probabilities for each condition are the same and the alternative that they are not. Performing McNemar test the null hypothesis is accepted (p=1,000 > 0,05); there is no significant difference in detection of accompanying sinonasal pathology between the pathological and healthy side.

Table 19. Accompanying sinonasal pathology in pathological and healthy sides.

		pathological side	
		0 (no sinonasal pathology)	1 (sinonasal pathology)
normal side	0 (no sinonasal pathology)	28	4
	1 (sinonasal pathology)	3	5
	McNemar Test	N=40	p-value= 1,000

Table 20 and graph 10 represent results of parametric independent sample t-test for Path_ETDQ7 and Path_ETS7 (scores of pathological sides) in cases of accompanying sinonasal pathology (presence or absence). The null hypothesis is that the mean values of the scores are equal, and the alternative that they are not. The mean value of Path_ETDQ7 in subjects which do not have accompanying sinonasal pathology (mean = 25,84) does not differ significantly (t(38) = 0,453, p = 0,653 > 0,05) from mean value of subjects which have (mean = 24,11). Furthermore, Path_ETS7 mean value of subjects which do not have accompanying sinonasal pathology (mean = 5,13) does not differ significantly (t(38)=-0,364, p=0,718>0,05) from mean value of subjects which have (mean = 5,56).

Table 20. Eustachian tube scores in presence/absence of accompanying rhinologic pathology in pathological sides.

Variables	Accompanying sinonasal pathology	N	Mean	df	t	p-value
Path_ETDQ7	absence	31	25,84	38	0,453	0,653
	presence	9	24,11			
Path_ETS7	absence	31	5,13	38	-0,364	0,718
	presence	9	5,56			

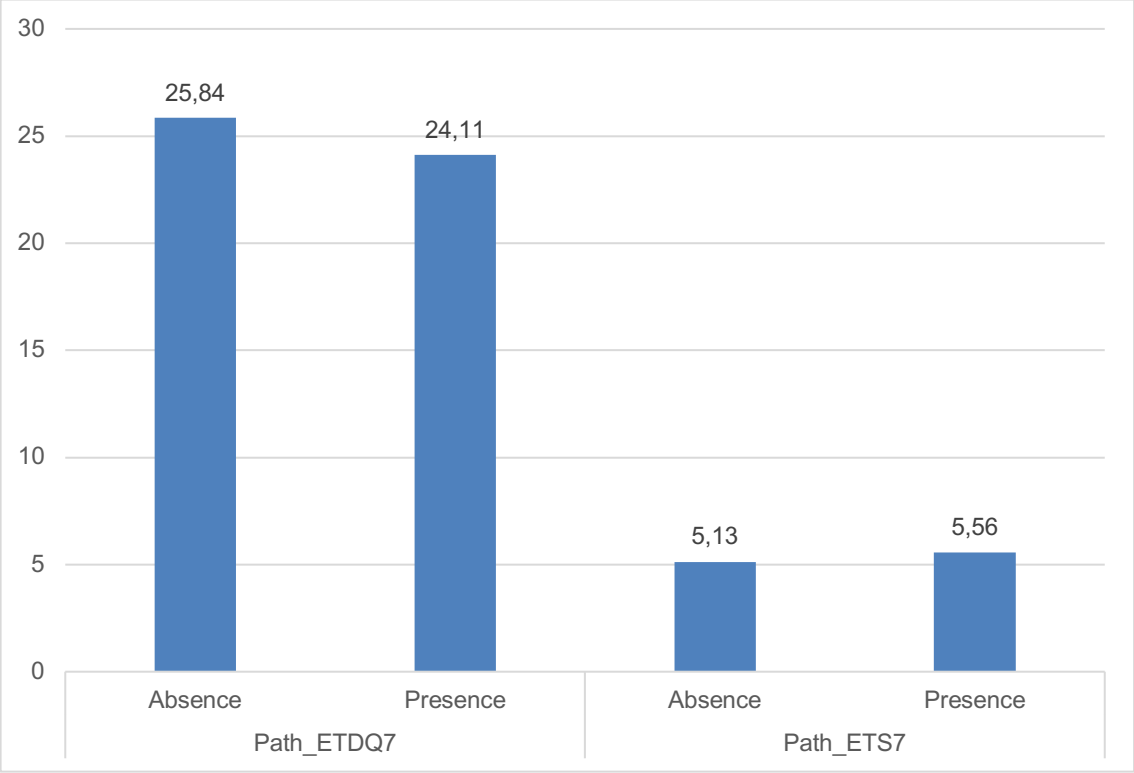

Graph 10. Mean values of Path_ETDQ7 and Path_ETS7 in presence/absence of accompanying sinonasal pathology in pathological sides.

Table 21 and graph 11 represent the results of parametric independent sample t-test for Path_ETDQ7 and Path_ETS7 (scores of pathological sides) in cases of accompanying sinonasal and otologic pathology (presence or absence of both conditions). The null hypothesis is that the mean values of the scores are equal, and the alternative that they are not. The mean value of Path_ETDQ7 in subjects

who do not have accompanying nose and ear pathology (mean = 25,57) does not differ significantly (t(38)=0,201, p= 0,842 > 0,05) from mean value of subjects who have both conditions (mean = 24,60). Moreover, Path_ETS7 mean value of subjects who do not have accompanying sinonasal and otologic pathology (mean = 5,26) doesn't differ (t(38) = 0,174, p = 0,863 > 0,05) from mean value subjects who have both conditions (mean = 5,00).

Table 21. Eustachian tube scores in presence/absence of accompanying sinonasal and otologic pathology on pathological sides.

Variables	Accompanying si-nonasal and otologic pathology	N	Mean	df	t	p-value
Path_ETDQ7	Absence	35	25,57	38	0,201	0,842
	Presence	5	24,60			
Path_ETS7	Absence	35	5,26	38	0,174	0,863
	Presence	5	5,00			

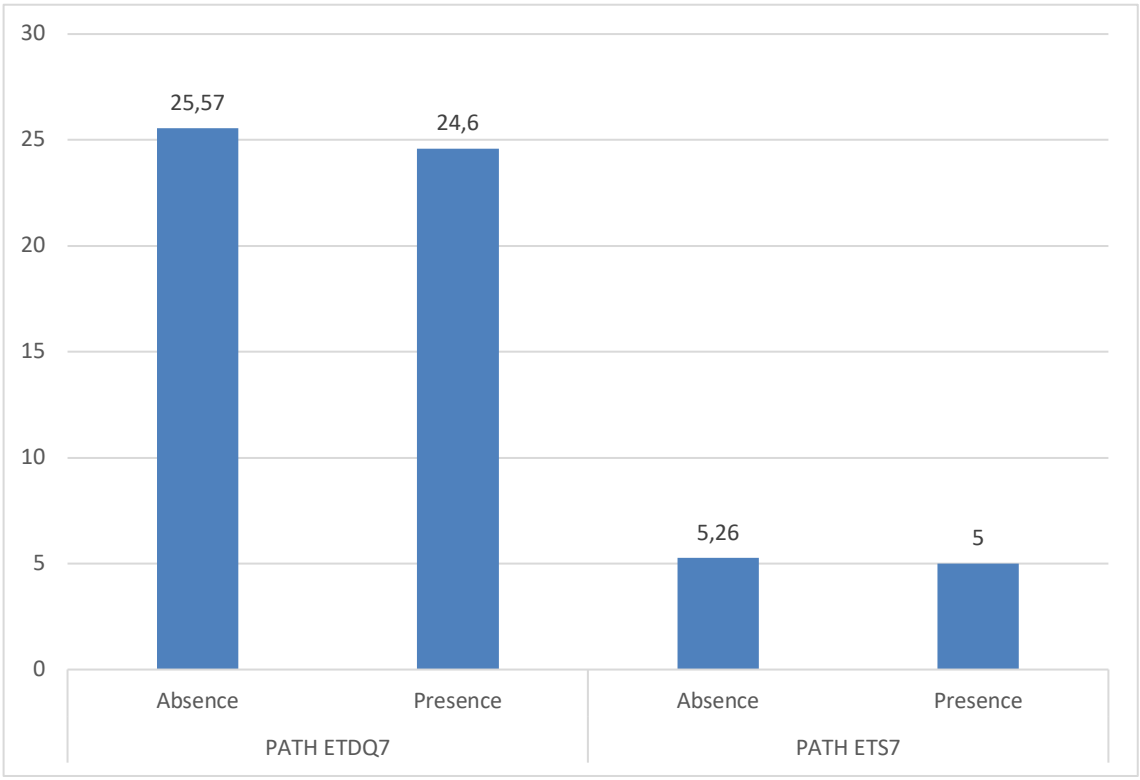

Graph 11. Mean values of Path_ETDQ7 and Path_ETS7 in presence/absence of accompanying sinonasal and otologic pathology on pathological sides.

3.2.4. 4th research aim

Is the radiological assessment of CT images a valid diagnostic tool for Eustachian tube dysfunction? What are the sensitivity, specificity, positive and negative predictive values of radiological evaluation?

Table 22 summarizes the results of radiologists' statement concerning the status of the Eustachian tube.

Table 22. Radiologists' statements concerning Eustachian tube dysfunction.

		Side of pathology (O)	
		Pathological (+)	Normal (-)
Radiologists' statement (R)	Pathological (+)	21	1
	Non-evaluable	18	18
	Normal (-)	1	21

In 21 of 80 tubes, the radiologists could correctly detect the pathologic side; the contralateral side was correctly characterized as healthy (21 of 80). In 1 of 80 tubes, they considered it pathological, but it was normal (false positive); the reverse happened for 1 of 80 tubes, that was considered normal but was pathologic (false negative). In 18 cases, i.e. in 36 of 80 tubes, the radiologists could not differentiate the side of pathology (non-evaluable cases). In these cases, the Eustachian tubes presented regularly.

Processing these results to determine the validity of radiologists' statement could be done with different approaches:

1. *“Intention to diagnose” principle [43] (Table 23)*

Table 23. “Intention to diagnose” principle.

		Side of pathology (O)	
		Pathological (+)	Normal (-)
Radiologists’ statement (R)	Pathological (+)	21	1+18=19
	~~Non evaluable~~	~~18~~ ↓	~~18~~ ↑
	Normal (-)	1+19=19	21

Sensitivity = $\frac{21}{21+19}$ = $\frac{21}{40}$ = 52,5 %

Specificity = $\frac{21}{21+19}$ = $\frac{21}{40}$ = 52,5 %

Positive predictive value = $\frac{21}{21+19}$ = $\frac{21}{40}$ = 52,5 %

Negative predictive value= $\frac{21}{21+19}$ = $\frac{21}{40}$ = 52,5 %

2. *Non-evaluable results considered to be healthy (Table 24)*

Table 24. “Non-evaluable results considered to be normal” approach.

		Side of pathology (O)	
		Pathological (+)	Normal (-)
Radiologists’ statement (R)	Pathological (+)	21	1
	~~Non evaluable~~	~~18~~ ↓	~~18~~ ↓
	Normal (-)	1+19=19	21+18=39

Sensitivity = $\frac{21}{21+19}$ = $\frac{21}{40}$ = 52,5 %

Specificity = $\frac{39}{39+1}$ = $\frac{39}{40}$ = 97,5 %

Positive predictive value = $\frac{21}{21+1}$ = $\frac{21}{22}$ = 95,4 %

Negative predictive value= $\frac{39}{19+39}$ = $\frac{39}{58}$ = 67,2 %

3. <u>Excluding non-evaluable cases (Table 25)</u>

Table 25. "Excluding non-evaluable cases" approach.

		Side of pathology (O)	
		Pathological (+)	Normal (-)
Radiologists' statement (R)	Pathological (+)	21	1
	~~Non-evaluable~~	~~18~~	~~18~~
	Normal (-)	1	21

Sensitivity = $\frac{21}{21+1}$ = $\frac{21}{22}$ = 95,4 %

Specificity = $\frac{21}{21+1}$ = $\frac{21}{22}$ = 95,4 %

Positive predictive value = $\frac{21}{21+1}$ = $\frac{21}{22}$ = 95,4 %

Negative predictive value= $\frac{21}{1+21}$ = $\frac{21}{22}$ = 95,4 %

4. Discussion

4.1. General considerations

The Eustachian tube represents a key factor for the proper function of the middle ear and subsequently hearing ability by its equalization, mucociliary drainage and protective functions. Impaired *Eustachian tube function* induces or contributes to the onset of frequent middle ear pathologies such as seromucous otitis, retraction process of tympanic membrane and cholesteatoma. Furthermore, its dysfunction probably leads to poor postoperative outcomes after performing middle ear surgery and forces the physician to perform revision procedures.

The development of novel therapeutical interventions for addressing Eustachian tube pathology in recent years, makes an accurate diagnostic tool even more essential. Minimal invasive techniques such as the *"balloon dilatation of the Eustachian tube (ETBD)"* [44] have already proven their efficacy. They are widely established as the first-line treatment for patients suffering from impaired function of the Eustachian tube (dilatory and baro-challenged induced Eustachian tube dysfunction) [45,46]. Nevertheless, establishing the correct diagnosis remains a challenge for the physician due to the lack of a gold standard diagnostic procedure [25].

Systematic reviews of Di Martino [47] and Smith et al. [28] showed that plenty of clinical tests for detecting Eustachian tube dysfunction have been applied in daily clinical practice in the past. However, up to now, none of them could provide an overall, detailed assessment of Eustachian tube physiology and pathophysiology. Patient questionnaires, such as the ETDQ-7 and ETS-7, represent a noninvasive and simple to use method to approach diagnostically pathological conditions and have gained much popularity in recent years [30-32, 48]. Especially the combination of both tests could lead to high diagnostic accuracy [28].

Besides, modern advances in imaging methods serve as an adjuvant workhorse for further understanding of Eustachian tube anatomy and function in the context

of Eustachian tube dysfunction [29]. The ideal radiological test should be simple, fast, non-invasive, low-cost and providing not only statical, anatomic information but also dynamic, functional aspects of tubal function. CT and MRI as radiological investigations could detect features associated with some form of Eustachian tube dysfunction [55-59, 71], *"though more reliable assessment of function has only been achieved using contrast-enhanced radiography or scintigraphy" [29].* Till now, it is debatable whether the CT-scan should have a significant role in the preoperative diagnostic setting, or should apply for exceptional cases [49].

4.2. Cohort and imaging technique

In the present study, the cohort consisted of adult patients diagnosed with unilateral disease. This fact accommodated the advantage of having an internal control group and thus comparing radiologic findings between the pathological and healthy side. In this way, inter-individual differences in developmental and anatomical features could be minimized. The subjects presented with characteristic symptoms for Eustachian tube dysfunction (aural pressure, impaired hearing, "crackling" ear sounds and insufficient equilibration Valsalva manoeuvre) and nobody complained about sinonasal symptoms, such as nasal discharge, blocked nose, hyposmia or facial pain. Nevertheless, in 12/80 (15%) cases, ancillary sinonasal pathology could be identified (majorly chronic sinusitis of maxillary sinus with mucosa thickening, mucus or minor polyposis). Similar incidental sinus pathology rates have been reported by Ani et al. (23%) [50] and Ashraf et al. (Lund-MacKay CT score mean 4,26) [51] from the non-symptomatic population, showing that this condition is frequent.

The Valsalva-CT-technique was used to acquire the radiological dataset and assess the morphology of the Eustachian tube. The Eustachian tube is usually collapsed during the resting condition. Moreover, conventional CT scan does not offer the best possible contrast for evaluating the cartilaginous part (soft tissue). Therefore, the Valsalva-CT-technique was crucial to enhance the visualization of the lumen. According to Tarrabichi et al. [35], who proposed this technique in

2014, visualization of the entire length of cartilaginous part (approximately in 33% of cases) and significant increase of visualized length at the distal part of Eustachian tube (in 71/76 patients, i.e. 94%) could be achieved. In our setting, this technique has been applied easily during the short image acquisition times (spiral CT), did not demand extra equipment and did not add additional expenses to our setting. Alper et al. [52] recently used an analogous approach to visualize the Eustachian tube lumen by obtaining CT-scan images during the forced response test (standardized pressure application in the nasopharynx), indicating an increased interest to find a practical way to gain more radiological information about this complex organ.

As mentioned before, the radiologic evaluation was performed independently by two neuroradiologists. For reliability, the Intraclass Correlation Coefficient [ICC: two-way mixed-effects model, absolute agreement, average measures] showed excellent inter-rater variability between the two physicians (ICC .991, F(212)=114,484, p=.000<.001) [53].

4.3. Morphological measurements

The cross-sectional size of the pharyngeal and tympanic orifice of Eustachian tube

There was a significant moderate positive correlation between Eustachian tube score ETS-7 and the cross-sectional size of tympanic orifice (S2) (r=0,361, p<0,05, Pearson) according to Cohen [54]. A bigger cross-sectional size of the tympanic orifice (S2) correlates with higher scores of ETS-7, indicating a better ventilation or pressure equalization function of the Eustachian tube. Similar results were found in previous studies; a reduced cross-sectional area of the tympanic segment correlated with the pathologic group compared to healthy individuals (summary in Table 26). Measuring the tympanic orifice could be a specific imaging feature indicating obstructive Eustachian tube dysfunction and thus could be integrated into a preoperative evaluation protocol.

Table 26. Tympanic cross-sectional size as a predictive radiologic feature of Eustachian tube dysfunction, COM: Chronic Otitis Media, ETD: Eustachian tube dysfunction.

Article	Cohort characteristics	Core findings
Conticello et al. [55] 1989	• COM (n unknown), • controls (healthy subjects, n unknown)	Constricted lumen found in COM
Yoshida et al. [56] 2007	• 38 COM/obstructive ETD • 40 controls (healthy subjects)	Smaller bony framework found in COM/obstructive ETD
Shim et al. [57] 2010	• 80 COM ad tympanoplasty • 100 controls (healthy subjects)	The small mean cross-sectional area corresponds to poor aeration subgroup
Paltura et al. [58] 2016	• 232 COM/ETD (unilateral) • 232 internal controls (contralateral ears)	The bony diameter of ET less in COM/ETD side
Nemade et al. [59] 2018	• 92 COM • 108 controls (healthy subjects)	ET pre-tympanic diameter significantly less in COM patients

There was no correlation between Eustachian tube scores (ETDQ7 and ETS7) and the cross-sectional size of pharyngeal orifice (S1). Terzi et al. have reported the only coinciding literature data evidence in 2016 [60], who performed MRI-morphologic measurements: the mean diameter of the pharyngeal orifice was not significantly different between the pathological and normal sides in 40 patients with suppurative otitis media (internal control group).

Visualization of the Eustachian tube lumen

A significant difference was detected between normal and pathological sides in terms of visualization of Eustachian tube lumen. Particularly, the mean value of visualization grade of complete Eustachian tube (V1) and in its' bony segment (V3) was higher in healthy sides rather than in pathological sides [$Z = -2{,}124$, $p = 0{,}034 < 0{,}05$ / $t(39) = 2{,}427$, $p = 0{,}020 < 0{,}05$ and $Z = -2{,}177$, $p = 0{,}029 < 0{,}05$ and $t(39) = 2{,}817$, $p = 0{,}008 < 0{,}05$ respectively]. Moreover, correlation between Eustachian tube score ETS-7 and visualization length of complete Eustachian tube (V1) and in its' bony segment (V3) could be identified. The degree of correlation between ETS7 and V1 (Dif_ analysis: $r=0{,}436$, $p<0{,}01$, Pearson / Path_ analysis: $r=0{,}382$, $p<0{,}05$, Spearman) could be considered as moderate to strong and the correlation between ETS7 and V3 (Dif_ analysis, $r=0{,}598$, $p<0{,}01$, Spearman) strong [54]. Greater visualization of the Eustachian tube on CT scans acquired whilst performing a Valsalva maneuver is correlated with either higher scores of ETS-7 or a bigger difference of scores of the healthy and pathological side. Both conditions are reflecting a better function of the Eustachian tube.

Evidence of analogous correlation could not be identified after comprehensive literature research in various clinical databanks (e.g. PubMed or Medline) till to date. This could be due to difficulties of visualization of the Eustachian tube through conventional computer tomography. The simultaneously applied Valsalva manoeuvre provides the advantage of maximizing visualization, especially of the *distal part (cartilaginous part) of the Eustachian tube*, which is physiologically collapsed and therefore not visible on CT-scan [35]. A study from 2007 [61] has been performed on subjects with patulous Eustachian tubes and revealed a significant difference of open tubal distance (equivalent to visualization grade in the current study) in the pathologic group versus the control group, confirming that *"more visualized air space in the Eustachian tube correlates with a better ventilation function".* Various research groups reported implementations to delineate Eustachian tube lumen using MRI-imaging protocols for better soft-tissue contrast [60, 62, 63]; limitations of these studies comprised either small case

numbers or inconsistent reporting of correlation between radiological findings and function tests of Eustachian tube.

The strong correlation between the visualized bony segment and the scores supports our previous hypothesis (s. page 47) that measurements of the osseous part could offer us reliable predictive factors of proper Eustachian tube function. This statement comes in agreement with increasing endoscopic and histopathologic evidence, concerning the essential pathophysiologic, obstructive role of the tympanic segment in the genesis of Eustachian tube dysfunction and subsequent middle ear pathologies [64-66].

Eustachian tube angles

It is generally alleged that Eustachian tube's shorter length and shallower angle to the skull base in childhood [18,19] is a major predisposing factor for reduced ventilation of middle ear cavity/mastoid, causing a higher prevalence of recurrent otitis media in this age group compared to adults [67,68].

Results in the present study demonstrate that Eustachian tube scores ETDQ-7 and ETS-7 are not correlated with the Eustachian tube inclination angle to the Francfort horizontal plane (Ia) [42]. A more horizontal position or swallower angle does not correlate with weak function in adults. This fact comes in agreement with conclusions of other authors, who described non-significant differences in inclination angle between healthy and diseased subjects (Table 27a). Only Tsai et al. [71], who compared ten ears (cholesteatoma) with the contralateral healthy side, found a significantly higher Eustachian tube angle in healthy ears (Table 27b).

Table 27. The inclination angle of Eustachian tubes as a predictive radiologic feature of Eustachian tube dysfunction, **a**: no correlation, **b**: correlation, OME: Otitis Media with effusion, COM: Chronic Otitis Media

a.

Article	Cohort characteristics	Core findings
Takasaki et al. [18] 2007	• 54 OME in children • 50 controls, children without OME (healthy subjects)	No significant difference of Eustachian tube angle between OME and healthy children group
Dinc et al. [19] 2015	• 62 COM (Tympanosclerosis, retraction process, cholesteatoma) • 62 internal controls (contralateral ears)	No significant difference in Eustachian tube angle between the pathological and normal side
Yegin et al. [69] 2016	217 ears in 3 groups of different grades of mastoid pneumatization (CT-morphologically)	Eustachian tube angle is not significantly different throughout the three groups
Yegin et al. [70] 2017	Group A Tympanoplasty • 39 good postop. outcomes • 39 internal controls (contralateral ears) Group B Tympanoplasty • 12 poor postop. outcomes • 12 internal controls (contralateral ears)	No differences of Eustachian tube angle between groups as well as pathological-normal side

b.

Article	Cohort characteristics	Core findings
Tsai et al. [71] 2010	10 attic cholesteatoma 10 internal controls (contralateral ear)	Eustachian tube angle significantly higher in healthy sides

The shape, volume and consistency of Eustachian tube has been investigated thoroughly either by histopathological [22, 72] or radiological methods [38], and both showed excellent interindividual and age variance. For the first time in this study, we investigated the curvature angle of the Eustachian tube (Ca) and correlated it with the *Eustachian tube scores*. This angle indicates how curved or flattened a Eustachian tube is [36]. No significant correlation could be found between different degrees of curvature and Eustachian tube scores.

Predictive models

Multiple, linear regression was performed to assess the ability of morphologic measurements (independent variables) to predict *Eustachian tube scores* (depended on variables). Following models have been constructed:

1. Dif_ETS7= 4,08 + 0,09 x Dif_V3 – 0,39 x Dif_Ca

2. Path_ETS7= 0,16 + 0,04 * Path_V3 + 0,2 * Path_ S2

The Adjusted R^2-values were 0,384 and 0,241 for the model (1) and (2) respectively, indicating a low (to almost moderate) strength to predict the variance of Dif_ETS7 and Path_ETS7 using as predictors Dif_V3/Dif_Ca and Path_V3 /Path_S2. Merely 38% of the variance of the response data can be explained by the model (1) and 24% for the model (2), demonstrating no significance for daily clinical practice.

4.4. Co-factors of disease

Although numerous studies evaluated the probability of a causal relationship between sinonasal pathology (i.e. acute or chronic rhinosinusitis) and *Eustachian tube dysfunction* in different ways (endoscopy findings, tympanometry, audiometry, tube ventilation tests), the clinical prevalence of this condition in patients is

yet uncertain [73]. The current established theory postulates that the inflammatory disease of the nose negatively affects the function of Eustachian tube due to mucosal oedema (obstruction) and posterior sinonasal discharge (ascending infection) [74]; the mucociliary clearance and pressure-equilibration is consequently disturbed, giving rise to otologic symptoms (e.g. ear pressure, impaired hearing). The recognition of *Eustachian tube dysfunction* as a comorbidity of rhinosinusitis is also reflected in the fact that widely used patient-reported rhinosinusitis scores such as the *"Sino-Nasal Outcome Test – 22*" integrate otologic symptoms (*"SNOT - 22 ear subdomain: ear fullness, dizziness, ear pain, facial pain/pressure")* [75]. A recent study showed a significant correlation between Eustachian tube dysfunction score ETDQ-7 and SNOT-22, especially with its ear subdomain [76], implying a cause-effect relationship between the two conditions. However, this study could not find a correlation between ETDQ-7 and Lund-Mackay CT score (staging score based on radiological findings of sinusitis) and Lund-Kennedy endoscopy score (staging score based on endoscopic evidence of sinus disease).

In the present study we assessed primarily, if the ancillary detection of rhinologic pathology (i.e. sinus pathology) in CT-scans concords with the pathologic side (tubal impairment). We found no association between radiological findings of sinus disease and side of Eustachian tube dysfunction (Mc Nemar, p=1,000>0,.05). Secondary, mean values of *Eustachian tube scores* ETDQ-7 and ETS-7 did not differ between sides with or without adjacent sinus pathology (independent sample t-test, t(38) = 0,453, p = 0,653 > 0,05 and t(38)=-0,364, p=0,718>0,05 respectively). Even in cases of accompanying sinonasal and ear pathology (radiological and clinical findings), the *Eustachian tube scores* mean values didn not differ (independent sample t-test, t(38)=0,201, p= 0,842 > 0,05 and t(38) = 0,174, p = 0,863 > 0,05 respectively). This discrepancy between objective radiological findings and subjective symptoms appears consistent with the disclosures of Tangbumrungtham et al [76]: radiologic detection of rhinologic pathology cannot be considered as a valid predictor to identify *Eustachian tube dysfunction.*

One of the main Eustachian tube functions is the descending mucociliary clearance of secretions from middle ear cavity and mastoid cell system towards the nasopharynx [9]. Also, the mucosal lining of the Eustachian tube itself contains goblet cells which produce mucus capable of immunologic and transport properties [77]. Pathologic thickening of mucosa and excessive hyperplasia of goblet cells lead to increased production of mucus that may obstruct the Eustachian tube and compromise middle ear cleft ventilation [66, 77]. Especially in its narrowest part, the isthmus, the impact of this condition could be enormous [65].

In contrary to sinonasal pathology, in our study, the radiologic detection of mucus in Eustachian tube or adjacent middle ear cleft structures was associated with the pathologic Eusatchian tube function. Mucus was detected in 10 ears/tubes out of 80; all of them corresponded to the pathologic side (n=10/40; 25%). The healthy tubes did not have signs of mucus retention or mucosal thickening. This could be an indication, that *Eustachian tube dysfunction*, at least in some patients, is caused by a pathological mucociliary clearance.

4.5. The validity of radiologists' statement

Sensitivity, specificity, positive, and negative predictive values were calculated to evaluate the accuracy of radiologists in differentiating between pathologic and healthy Eustachian tubes using Valsalva-CT. The radiologists, who assessed the radiological dataset blinded to the side of diagnosis, could give a clear statement for 22 of 40 patients (55%). In 18 subjects (36 of 80 Eustachian tubes; 45%), the side of pathology could not be determined; this was due to symmetrical/equal presentation of Eustachian tubes on both sides and absence of any pathologic criteria (for example stenosis) and the subjective difference in visualization grade, posture or shape. Adjacent anatomic structures were without pathologic findings. Therefore, these Eustachian tubes were characterized primarily as non-evaluable, but practically, presented as normal/healthy-appearing Eustachian tubes.

Different approaches were used to assess the data of the 3x2 Table, including the non-evaluable results (s. chapter “Results”, Table 22, page 42). The sensitivity of radiologists’ evaluation was 52,5 % regardless of method (“intention to diagnose principle” [43] and “non-evaluable considered normal approach”). The specificity, however, showed differentiation between the two methods: it was 52,5% and 97,5% respectively.

The approach “non-evaluable considered to be normal” is reflecting the standard condition in our study, since the radiologists labelled actually normal Eustachian tubes as non-evaluable results. The probability of correctly detecting the pathologic side is low (sensitivity 52,5%). That practically means, if the radiologist would see a regular Eustachian tube, he could rule out a pathologic tube with a probability of 52,5%. On the other hand, detecting correctly a normal Eustachian was much more probable (specificity 97,5%). Consequently, if the radiologist saw a pathologic Eustachian tube, he would establish the diagnosis of a diseased tube in 97,5%. Looking at the third approach, where non-evaluable cases were excluded, we can conclude that the radiologist had an excellent performance in detecting pathologic and healthy sides. In other words, if the radiologist could give a definite statement, then it would be probably correct. These results are following positive and negative predictive values. The following Table summarizes the results (Table 28).

Table 28. Diagnostic value of radiologic evaluation of Eustachian tubes, “non-evaluable considered normal” approach.

Sensitivity = 52,5 %	Positive predictive value = 95,4 %
Specificity = 97,5 %	Negative predictive value= 67,2 %

4.6. Limitations

Patients who have been included in the present study had an age ranging from 17 to 87. Children were excluded from CT-scanning because of X-ray hazard and

no proven diagnostic benefit [49] even though this particular patient population seems to have the highest prevalence of Eustachian tube dysfunction [26]. An age-related data analysis could not be conducted because of the modest case number. Even though the development of the Eustachian tube is completed at the age of 7 [78], further age-related changes of Eustachian tube due to calcification of soft tissue degeneration are not clarified yet [36,72]. Such developmental changes could have a great impact on Eustachian tube function.

Twenty out of forty patients had an accompanying ear pathology such as middle ear effusion or tympanic membrane retraction. Since the *"interaction between middle ear disease and eustachian tube pathology is poorly understood"* [79], this fact could influence our results. Furthermore, systemic comorbidities, such as gastroesophageal reflux have not been taken into account [80].

All Valsalva-CT-scans were acquired in the supine/recumbent position. This method has the handicap of venous/lymphatic blood congestion in peri-tubal soft tissue [41]. This condition consequently enhances the physiological collapse and reduces the patency of the already thin, cleft shaped Eustachian tube lumen. Evidence in the literature indicates that air space in cartilaginous Eustachian tube lumen is larger in CT-scans acquired in the sitting position than in recumbent position; a significant difference does not exist at the bony part [41,61]. On the other hand, performing a CT-scan in sitting position demands a cone-beam CT system setting which is not widely available and established as the conventional one.

Patients were thoroughly instructed on how to perform a Valsalva manoeuvre simultaneously to CT scan by experienced technicians who underwent a 3-month instruction period before data collection to optimize the investigation protocol. Nevertheless, we consider a bias source due to poor Valsalva technique, at equivalent rates as Tarabichi et al. [35] have reported previously (approx. 3%). A standardization of applied pressure in nasopharynx for opening would be favourable.

4.7 Future considerations

Imaging evaluation of the Eustachian tube is gaining renewed interest since new therapeutic approaches to resolve its dysfunction have been introduced to clinical practice during the last years [29]. As shown in this study, conventional radiologic methods, which rely on static image acquisition (i.e. standard CT or MRI), cannot evaluate functional aspects of Eustachian tube and hence have faced critical reviews [29, 49, 81]. Invasive or complex imaging methods like radiographic and scintigraphy tests could not be introduced into practicable clinical practice despite a possible potential [29]. The ultimate goal of establishing a golden standard radiologic technique may be achieved by focusing on dynamic imaging techniques. Cine computed tomography protocols [82,83] and functional MR imaging [63] have presented promising results, although large scale trials have not been implemented yet to prove their applicability. Advanced volume rendering protocols could be applied to generate 3D models [29], which could then be correlated to different pathologic conditions. This combination of dynamic imaging and 3D-reconstruction may perhaps help to clarify *Eustachian tube dysfunction.*

4.8. Conclusion

The current study examined whether morphological measurements of Eustachian tube in images obtained by Valsalva-CT scan are correlated with clinical Eustachian tube scores and tried to clarify the value of radiologic assessment of the Eustachian tube and adjacent middle ear and nose structures in the diagnostic workup. The results show that the radiologic evaluation of Eustachian tube could provide us with detailed anatomic information about its complex structure but is insufficient to yield reliable data about its function. In addition, the sensitivity of radiologic assessment is rather low and hence is inappropriate as a screening tool for Eustachian tube dysfunction in daily clinical use. The x-ray exposure, the low predictive value and aspects of healthcare economics are not justifying using computed tomography of the temporal bone for routine diagnostic evaluation. The acquisition of CT-scan images should be reserved for individual enquiries such

as history of skull base trauma, congenital or developmental abnormalities, tumour suspicion and revision surgery of Eustachian tube. If a patient presents with CT-scans of the temporal bone, then the focus of attention should be laid on the tympanic segment and the detection of mucus in the Eustachian tube or adjacent structures.

5. Abstract

Objectives

i. Investigate whether morphologic measurements of Eustachian tubes on *computed tomography scans* are correlated with Eustachian tube dysfunction scores.
ii. Investigate whether sinonasal or middle ear radiological findings on temporal bone computed tomography are associated with the side of Eustachian tube dysfunction.
iii. Determine the diagnostic validity of the *computed tomography scan* as a screening tool for *Eustachian tube dysfunction*.

Study design

Prospective, cross-sectional case series study in a tertiary referral centre (ViDia Christian Hospitals Karlsruhe).

Methods

The study included forty patients with clinically diagnosed unilateral Eustachian tube dysfunction, verified through Eustachian tube score – 7 and Eustachian tube dysfunction questionnaire – 7.

Each patient underwent pre-interventional radiological assessment by temporal bone computed tomography while performing a Valsalva-maneuver to enhance visualization of Eustachian tube lumen. The complete course of Eustachian tube, from the epipharynx to the middle ear cleft was included in the scanning field.

A curved planar reconstruction delineated the Eustachian tubes and 3D models were constructed using volume rendering software. Seven morphological parameters were independently measured for each Eustachian tube by two board-certified neuroradiologists blinded to the side of pathology: the cross-sectional size of the tympanic and pharyngeal orifice, visualization length of cartilaginous, bony

and overall Eustachian tube lumen as well as inclination angle to Frankfurt horizontal plane and curvature angle of the S-shaped Eustachian Tube. Furthermore, the Eustachian tubes were analyzed for inter-side morphological differences, presence of mucus in the lumen or middle ear cleft and secretion retention or mucosal swelling in the adjacent sinuses. Finally, a radiological statement about the side of pathology was delivered, always blinded to the clinical diagnosis.

Statistical correlation studies between morphological measurements and Eustachian tube scores analyzed the association between the presence of mucus or accompanying sinonasal disease. Additionally, the diagnostic validity of the computed tomography scan as a screening tool for Eustachian tube dysfunction was calculated.

Results

There was no significant correlation between Eustachian tube scores and the cross-sectional size of pharyngeal orifice. On the other side, correlation between Eustachian tube score - 7 and the cross-sectional size of tympanic orifice could be identified ($r=0,361$, $p<0,05$, Pearson). The mean value of visualization length of complete Eustachian tube and in its' bony segment was higher in healthy sides rather than in pathological sides [$Z = -2,124$, $p = 0,034 < 0,05$ / $t(39) = 2,427$, $p = 0,020 < 0,05$ and $Z = -2,177$, $p = 0,029 < 0,05$ and $t(39) = 2,817$, $p = 0,008 < 0,05$ respectively]. Moreover, correlation between Eustachian tube score - 7 and visualization length of complete Eustachian tube and in its' bony segment could be identified ($r=0,462$, $p<0,01$, Pearson and $r=0,598$, $p<0,01$, Spearman respectively). No significant correlation could be found between different grade of inclination/curvature and Eustachian tube scores.

The radiologic detection of mucus in Eustachian tube or adjacent middle ear cleft structures was associated with the pathological side. On the contrary, there is no association between radiological findings of sinus disease and side of Eustachian tube dysfunction.

The diagnostic value of radiologic assessment in Eustachian tube dysfunction has a sensitivity of 52,5 and specificity of 97,5%.

Conclusion

Measuring the tympanic orifice could be a specific imaging feature indicating obstructive Eustachian tube dysfunction and thus could be integrated into a preoperative radiological evaluation protocol. The sensitivity of radiologic assessment is rather low. Hence, Valsalva-CT is inappropriate as a screening tool for Eustachian tube dysfunction in routine clinical practice. However, the presence of mucus in Eustachian tube or adjacent structures on temporal bone CT scan is the most specific morphologic correlate to Eustachian tube dysfunction.

Savvas Kourtidis, 01.04.2020

Prof. Dr. med. Serena Preyer, 01.04.2020

- German Translation of Abstract -

Ziele der Studie

i. Korrelation zwischen computertomographischen, morphologischen Messungen der Tuba Eustachii und den Tubenventilationsstörung-Scores.
ii. Assoziation zwischen radiologischen Nebenbefunden der Nasennebenhöhlen oder des Mittelohrs und der Seite der Tubenventilationsstörung.
iii. Diagnostische Validität der computertomographischen Untersuchung der Tuba Eustachii als “screening tool” für die Tubenventilationsstörung.

Studiendesign

Prospektive, Fall-Kontroll-Studie in einem Tertiärzentrum (ViDia Christliche Kliniken Karlsruhe)

Methodik

In die Studie wurden vierzig Patienten mit einer klinisch diagnostizierten, unilateralen Tubenventilationsstörung eingeschlossen. Die Diagnosen wurden durch die Tubenventilationsstörung-Tests “Eustachian tube score – 7” und “Eustachian tube dysfunction questionnaire – 7” verifiziert.

Jeder Patient bekam routinemäßig eine Computertomographie der Felsenbeine beiderseits. Die Durchführung eines Valsalva-Manövers während der Computertomographie steigerte die Visualisierung der Tuba Eustachii. Der gesamte Verlauf der Tuba Eustachii wurde abgebildet, vom Epipharynx bis hin zum Mittelohr.

Durch “Curved Planar Reconstruction” konnten die Tuben dargestellt werden und durch “Volume Rendering” konnten 3D Modelle erstellt werden. Sieben morphologische Parameter für jede Tube wurden von zwei erfahrenen Neuroradiologen, unabhängig und verblindet zu der klinischen Diagnose ausgewertet: die Querschnittsfläche des pahryngealen und tympanalen Tubenostiums, die Länge der visualisierten Tube im gesamten, knorpeligen und knöchernen Anteil, der

Inklination Winkel zu der Frankfurter Horizontale und der Kurvatur Winkel der S-förmigen Tuba Eustachii. Zusätzlich wurden Nebenpathologien in der Nase/Nasennebenhöhlen und im Mittelohr beurteilt. Anschließend mussten die Neuroradiologen, die verblindet zu der klinischen Diagnose waren, entscheiden, welche Seite pathologisch aussah.

Die statistische Auswertung der morphologischen Messungen und der Ergebnissen der Tubenventilationsstörung-Scores erfolgte mit Korrelationskoeffizienten. Die Assoziation zwischen Nebenbefunden (Nase, Nasennebenhöhlen, Mittelohr) und pathologische Seite wurde erforscht. Die diagnostische Aussagekraft der computertomographischen Untersuchung der Tuba Eustachii als “screnning tool” für Tubenventilationsstörung wurde evaluiert.

Ergebnisse

Eine signifikante Korrelation zwischen “Eustachian tube score – 7” und Querschnittfläche des tympanalen Tubenostiums konnte identifiziert werden ($r=0,361$, $p<0,05$, Pearson). Der Mittelwert der visualisierten Länge der Tuba Eustachii sowohl der gesamten Länge als auch im knöchernen Anteil war höher auf der gesunden Seite als auf der pathologischen Seite [$Z = -2,124$, $p = 0,034 < 0,05$ / $t(39) = 2,427$, $p = 0,020 < 0,05$ und $Z = -2,177$, $p = 0,029 < 0,05$ und $t(39) = 2,817$, $p = 0,008 < 0,05$ entsprechend]. Eine Korrelation zwischen den Ergebnissen des “Eustachian tube score – 7” und der Länge der Visualisierung sowohl der gesamten Länge als auch des knöchernen Anteils der Tuba Eustachii konnte identifiziert werden ($r=0,462$, $p<0,01$, Pearson and $r=0,598$, $p<0,01$, Spearman entsprechend).

Der radiologische Befund von Mukus in der Tuba Eustachii oder im angrenzenden Mittelohr (Protympanon) war assoziiert mit der pathologischen Seite. Im Gegensatz dazu, gab es keine Assoziation zwischen Nasenpathologie und Seite der Tubenventilationsstörung.

Die diagnostische Aussagekraft der computertomographischen Beurteilung der Tuba Eustachii bezüglich Tubenventilationsstörung beträgt eine Sensitivität von 52,5% und eine Spezifität von 97,5%.

Schlussfolgerungen

Lediglich die Detektion von Mukus in der Tuba Eustachii oder im angrenzenden Mittelohr (Protympanon) scheint ein radiologisches Merkmal zu sein, das gut mit der pathologischen Seite assoziiert ist. Die Sensitivität der computertomographischen Untersuchung ist eher mäßig und ist deshalb als primäres diagnostisches Verfahren bei der Diagnostik der Tubenventilationsstörung nicht geeignet. Die Abklärung einer Tubenventilationsstörung allein stellt keine rechtfertigende Indikation für die Durchführung einer Computertomographie des Felsenbeins dar.

Savvas Kourtidis, 01.04.2020

Prof. Dr. med. Serena Preyer, 01.04.2020

6. References

1. Stevenson S, Guthrie D (1949) A History of Oto-Laryngology. Livingstone, Edinburgh.
2. Eustachius B (1564) Epistola de auditus organis. In: Opuscula Anatomica. Luchinus, Venice.
3. O'Malley C (1971) Bartolommeo Eustachi: an epistle on the organs of hearing. An annotated translation. Clio Med 6(1): 49-62.
4. Valsalva A (1704) De Aure Humana Tractatus. Bononiae, Pisarii.
5. Canalis R. (1990) Valsalva's contribution to otology. Am J Otolaryngol 11: 420-427.
6. Duverney GJ (1737) A Treatise of the organ of hearing. Baker, London. Reprint: AMS Press, New York.
7. Politzer A (1883) A Textbook of the Diseases of the Ear and Adjacent Organs. Lea, Philadelphia.
8. Toynbee J (1860) The Diseases of the Ear: Their Nature, Diagnosis and Treatment. Churchill, London.
9. Bluestone C, Bluestone M. (2005) Eustachian tube: structure, function, role in otitis media. p. 113-150. Hamilton; Lewiston, BC Decker, New York.
10. Poe D et al. (2000) Analysis of Eustachian tube function by video endoscopy. Am J Otol 21(5): 602-607.
11. Poe D et al. (2003) Analysis of the dysfunctional eustachian tube by video endoscopy. Otol Neurotol 22: 590-595.
12. Ars B. (2003) Balance of pressure variations in the middle ear cleft; p. 57-66. In: Ars B (editor). Fibrocartilaginous eustachian tube – middle ear cleft. Kugler Publications, The Hague, The Netherlands.
13. Ars B, Dirckx J (2016) Eustachian Tube Function. Otolaryngol Clin North Am 49: 1121-33.
14. Rüdinger N (1870) Beiträge zur vergleichenden Anatomie und Histologie der Ohrtrompete. JJ Lentner'sche Buchhandlung, München.
15. Proctor B (1967) Embryology and Anatomy of the Eustachian tube. Arch Otolaryngol 86: 503-514.
16. Takasaki et al. (2002) Functional anatomy of the tensor veli palatini muscle and Ostmann's fatty tissue. Ann Otol Rhinol Laryngol. 111: 1045-9.
17. Zöllner F (1942) Anatomie, Physiologie, Pathologie und Klinik der Ohrtrompete und ihre diagnostisch-Therapeutischen Beziehungen zu allen Nachbarschaftserkrankungen. In: Hals-, Nasen-, Ohrenheilkunde der Gegenwart und ihre Grenzgebiete. Springer, Berlin.
18. Takasaki K et al. (2007) Measurement of Angle and Length of the Eustachian Tube on Computed Tomography Using the Multiplanar Reconstruction Technique. Laryngoscope 117: 1251-1524.

19. Dinc AE et al. (2015) Do the angle and length of the Eustachian tube influence the development of chronic otitis media? Laryngoscope 125: 2187–2192.
20. Kamimura M et al. (2001) Mucosa-associated lymphoid tissue in middle ear and eustachian tube. Ann Otol Rhinol Laryngol. 110: 243-247.
21. Rich A (1920) A physiological study of the Eustachian tube and its related muscles. Bull. Johns Hopkins Hosp 31: 3005-3010.
22. Proctor B (1973) Anatomy of the Eustachian tube. Arch Otolaryngol 97: 2-8.
23. Rood S, Doyle J (1978) Morphology of tensor veli palatine, tensor tympani and dilatator tubae muscles. Ann Otol Rhinol Laryngol 87: 202-210.
24. Ishijima K et al. (2000) Length of the Eustachian tube and its postnatal development: computer-aided three-dimensional reconstruction and measurement study. Ann Otol Rhinol Laryngol 109: 542–548.
25. Schilder AGM et al. (2015) Eustachian tube dysfunction: consensus statement on definition, types, clinical presentation and diagnosis. Clin Otolaryngol 40: 407-411.
26. Browning GG, Gatehouse S (1992) The prevalence of middle ear disease in the adult British population. Clin Otolaryngol Allied Sci 17: 317-321.
27. Norman G et al. (2014) Systematic review of the limited evidence base for treatments of Eustachian tube dysfunction: a health technology assessment. Clin. Otolaryngol 39: 6-21.
28. Smith ME, Tysome JR (2015) Tests of Eustachian tube function: a review. Clin Otolaryngol. 40: 300-311.
29. Smith ME et al. (2016) Imaging of the Eustachian tube and its function: a systematic review. Neuroradiol 58: 543-556.
30. McCoul ED et al. (2012) Validating the clinical assessment of Eustachian tube dysfunction: the Eustachian Tube Dysfunction Questionnaire (ETDQ7). *Laryngoscope* 122: 1137–1141.
31. Roeyen SV et al. (2015) Value and discriminative power of the seven-item Eustachian tube dysfunction questionnaire. *Laryngoscope* 125: 2553-2556.
32. Schröder S et al. (2015) A novel diagnostic tool for chronic obstructive eustachian tube Dysfunction-The eustachian tube score. Laryngoscope 125: 703-708
33. Flohr TG et al. (2007) Novel ultrahigh resolution data acquisition and image reconstruction for multi-detector row CT. Med Phys 34: 1712-1723.
34. Siemens Healthcare. ADMIRE – Advanced Modeled Iterative Reconstruction [cited 2019 Sep 01]. Available from: https://www.healthcare.siemens.de/computed-tomography/technologies-innovations/admire.
35. Tarabichi M, Najmi M (2014) Visualization of the eustachian tube lumen with Valsalva computed tomography. Laryngoscope 125: 724-729.
36. Kikuchi et al. (2009) Three-Dimensional Computed Tomography Imaging of the Eustachian Tube Lumen in Patients with Patulous Eustachian Tube. ORL 71: 312-316.

37. Ishijima K et al. (2002) Postnatal development of static volume of the eustachian tube lumen. A computer-aided three-dimensional reconstruction and measurement study. Ann Otol Rhinol Laryngol 111: 832-835.
38. Sudo M et al. (1998) Three-dimensional reconstruction and measurement study of human eustachian tube structures: a hypothesis of eustachian tube function. Ann Otol Rhinol Laryngol 107: 547-554.
39. Oberascher G, Grobovschek M (1987) The eustachian tube in HR computerized tomography. Imaging in the adult. Laryngol Rhinol Otol (Stuttg) 66: 605-609.
40. Yoshida H et al. (2003) CT imaging of the patulous eustachian tube - comparison between sitting and recumbent positions. Auris Nasus Larynx 30: 135-140.
41. Yoshida H et al. (2004) Imaging of the patulous Eustachian tube: high-resolution CT evaluation with multiplanar reconstruction technique. Acta Otolaryngol 124: 918-923.
42. Lanfermann H, Raab P, Kretschmann H-J, et al. (2015) Klinische Neuroanatomie - kranielle MRT und CT. Georg Thieme Verlag, Stuttgart.
43. Schuetz et al. (2012). Use of 3×2 Tables with an intention to diagnose approach to assess clinical performance of diagnostic tests: Meta-analytical evaluation of coronary CT angiography studies. BMJ 345: e6717.
44. Ockermann T et al. (2010) Balloon dilatation eustachian tuboplasty: a clinical study. Laryngoscope 120: 1411-1416.
45. Miller BJ, Elhassan HA (2013) Balloon dilatation of the Eustachian tube: an evidence-based review of case series for those considering its use. Clin Otolaryngol. 38: 525-532.
46. Poe D. et al. (2018) Balloon Dilation of the Eustachian Tube for Dilatory Dysfunction: A Randomized Controlled Trial. The Laryngoscope 128: 1200-1206.
47. Di Martino EF (2013) Eustachian tube function tests: an update. HNO 61: 467-76.
48. Schroeder S. et al. (2014) Assessment of chronic obstructive eustachian tube dysfunction: evaluation of the German version of the Eustachian Tube Dysfunction Questionnaire. HNO 62: 162-164.
49. Tisch M et al. (2013) Role of imaging before Eustachian tube dilatation using the Bielefeld balloon catheter. HNO 61: 488-491.
50. Ani CC et al. (2016) Incidental maxillary sinus findings on cranial computerized tomographic scan in a tropical setting. J West Afr Coll Surg 6: 39-51.
51. Ashraf N, Bhattacharyya N (2001) Determination of the “incidental” Lund score for the staging of chronic rhinosinusitis. Otolaryngol Head Neck Surg. 125: 483-6.
52. Alper CM et al. (2018) A Novel Imaging Method for the Cartilaginous Eustachian Tube Lumen: Computerized Tomography During the Forced Response Test. Ann Otol Rhinol Laryngol. 127: 13-20.
53. Koo TK, Li MY (2016). A Guideline of Selecting and Reporting Intraclass Correlation Coefficients for Reliability Research Journal of Chiropractic Medicine. 15: 155-63.

54. Cohen, J. (1988) Statistical Power Analysis for the Behavioral Sciences, 2nd ed. Erlbaum, Hillsdale – NJ.
55. Conticello S et al. (1989) Computed tomography in the study of the eustachian tube. Arch Otorhinolaryngol 246: 259-261.
56. Yoshida H et al. (2007) Anatomy of the bony portion of the eustachian tube in tubal stenosis: multiplanar reconstruction approach. Ann Otol Rhinol Laryngol 116: 681-686.
57. Shim HJ et al. (2010) The value of measuring eustachian tube aeration on temporal bone CT in patients with chronic otitis media. Clin Exp Otorhinolaryngol 3: 59-64.
58. Paltura C (2016) Eustachian tube diameter: Is it associated with chronic otitis media development? Otolaryngol. Head Neck Surg 38: 414-416.
59. Nemade SV (2018) Evaluation and significance of Eustachian tube angles and pretympanic diameter in HRCT temporal bone of patients with chronic otitis media. World J Otorhinolaryngol Head Neck Surg 4: 240-245.
60. Terzi A et al. (2016) The evaluation of eustachian tube paratubal structures using magnetic resonance imaging in patients with chronic suppurative otitis media, Acta Oto-Laryngologica 136: 673-676.
61. Kikuchi T (2007) Three-Dimensional Computed Tomography Imaging in the Sitting Position for the Diagnosis of Patulous Eustachian Tube. Otol Neurotol. 28: 199-203.
62. Krombach GA et al. (2000) Nuclear magnetic resonance tomography imaging and functional diagnosis of the eustachian auditory tube. Rofo 172: 748-752.
63. Lükens A et al. (2012) Functional MR imaging of the eustachian tube in patients with clinically proven dysfunction: correlation with lesions detected on MR images. Eur Radiol. 22: 533-538.
64. Tarabichi M, Najmi M (2015) Site of eustachian tube obstruction in chronic ear disease. Laryngoscope 125: 2572-2575.
65. Linstrom CJ et al. (2000) Eustachian tube endoscopy in patients with chronic ear disease. Laryngoscope 110: 1884-1889.
66. Christov F et al. (2019) Ballondilatation der Eustachischen Röhre (BET) – eine kritische Analyse. Laryngo-Rhino-Otol 98: 91.
67. Klein JO (1989) Epidemiology of otitis media. Pediatr Infect Dis J. 8: S9.
68. Qureishi A et al. (2014) Update on otitis media - prevention and treatment. Infect Drug Resist. 7: 15-24.
69. Yegin Y (2016) Correlation Between the Degree of the Mastoid Pneumatization and the Angle and the Length of the Eustachian Tube. J Craniofac Surg 27: 2088-2091.
70. Yegin Y (2017) Do the Angle and Length of the Eustachian Tube Affect the Success Rate of Pediatric Cartilage Type 1 Tympanoplasty? J Craniofac Surg. 28: e227-e231.
71. Tsai LT et al. (2010) Three-Dimensional Image Analysis of the Temporal Bone in Patients with Unilateral Attic Cholesteatoma. Neuroradiol Journal 23: 307-12.

72. Takasaki K (1999) Histopathological changes of the eustachian tube cartilage and the tensor veli palatini muscle with aging. Laryngoscope 109: 1679-83.
73. Stoikes NF, Dutton JM. (2005) The effect of endoscopic sinus surgery on symptoms of Eustachian tube dysfunction. Am J Rhinol. 19: 199-202.
74. Stammberger H (1986) An endoscopic study of tubal function and the diseased ethmoid sinus. Arch Otorhinolaryngol 243: 254-259.
75. Piccirillo JF et al. (2002) Psychometric and clinimetric validity of the 20-Item Sino-Nasal Outcome Test (SNOT-20). Otolaryngol Head Neck Surg 126: 41-47.
76. Tangbumrungtham N et al. (2018) The prevalence of Eustachian tube dysfunction symptoms in patients with chronic rhinosinusitis. Int Forum Allergy Rhinol. 8: 620-623.
77. Cayé-Thomasen P, Tos M (2003). Eustachian Tube Goblet Cell Density during and after Acute Otitis Media Caused by Streptococcus pneumoniae: A Morphometric Analysis. Otol Neurotol 24: 365-370.
78. Licameli GR (2002). The eustachian tube Update on anatomy, development and function. Otolaryngol Clin N Am 35: 803-809.
79. Tysome JR, Sudhoff H (2018) The Role of the Eustachian Tube in Middle Ear Disease. Adv Otorhinolaryngol. 81: 146-152.
80. Brunworth JD et al. (2014) Nasopharyngeal acid reflux and Eustachian tube dysfunction in adults. Ann Otol Rhinol Laryngol. 123: 415-419.
81. Abdel-Aziz et al. (2014) Computed Tomography Before Balloon Eustachian Tuboplasty – A True Necessity? Otol & Neurotol 35: 635-638.
82. McDonald M (2012) New insights into mechanism of Eustachian tube ventilation based on cine computed tomography images Eur Arch Otorhinolaryngol. 269: 1901-1907.
83. Jufas N (2016) Dynamic cine imaging of the Eustachian tube using four-dimensional computed tomography. J Laryngol Otol. 130: 1162-1164.
84. Yushkevich P et al. (2006) User-guided 3D active contour segmentation of anatomical structures: Significantly improved efficiency and reliability. Neuroimage 31: 1116-28.

7. Declaration of own work and contributions

I am declaring, that the conception, conduction, evaluation, literature research and writing of this study is my work. Contributions are listed below:

- The study was conceived in corporation with Prof. Dr. med Serena Preyer, Director of the Otolaryngology, Head and Neck Surgery Department at ViDia Christian Hospitals, Karlsruhe, Germany.

- The trial was conducted at ViDia Christian Hospitals Karlsruhe (Diakonissenkrankenhaus) under the supervision of Prof. Dr. med Serena Preyer, Director of the Otolaryngology, Head and Neck Surgery Department.

- The clinical and radiological data were collected at the Otolaryngology, Head and Neck Surgery and Radiology Departments of ViDia Christian Hospitals Karlsruhe.

- The radiological data were processed in cooperation with Dr. med. Johann-Martin Hempel at the Department of Neuroradiology, University Hospital Tübingen, Germany.

- Methodic counselling for statistical analysis was received through Dr. Gunnar Blumenstock at the Institute for Clinical Epidemiology and Applied Biometry.

Savvas Kourtidis

Karlsruhe, 01.03.2020

- German Translation of Declaration of own work and contributions -

Ich versichere, dass die Konzeption, Durchführung, Evaluation, Literaturrecherche und Schreiben dieser Arbeit durch mich erfolgten. Beiträge zu dieser Studie werden nachfolgend gelistet:

- Die Konzeption der Studie erfolgte in Zusammenarbeit mit Prof. Dr. med Serena Preyer, Klinikdirektorin der Klinik für Hals-, Nasen- und Ohrenheilkunde der ViDia Kliniken Karlsruhe.

- Die Arbeit wurde in ViDia Kliniken Karlsruhe, Standort Diakonissenkrankenhaus unter Betreuung von Prof. Dr. med Serena Preyer, Klinikdirektorin der Klinik für Hals-, Nasen- und Ohrenheilkunde der ViDia Kliniken Karlsruhe, durchgeführt.

- Die Akquisition der klinischen und radiologischen Daten erfolgte in der Klinik für Hals-, Nasen- und Ohrenheilkunde und Radiologie der ViDia Kliniken Karlsruhe.

- Die Bearbeitung der radiologischen Daten wurde in Zusammenarbeit mit Dr. med. Johann-Martin Hempel (Facharzt für Radiologie, Schwerpunktsbezeichnung Neuroradiologie, Universitätsklinikum Tübingen) durchgeführt.

- Die statistische Auswertung erfolgte eigenständig. Die methodische Beratung des Instituts für Klinische Epidemiologie und angewandte Biometrie der Universität Tübingen wurde in Anspruch genommen. Die Beratung erfolgte durch Dr. Gunnar Blumenstock.

Savvas Kourtidis

Karlsruhe, den 20.01.2020

8. List of publications

At the time of the dissertation submission, the following articles are in review process for publication in medical journals:

1. Diagnostic value of computed tomography in Eustachian tube dysfunction

Authors
Savvas Kourtidis[a], Johann-Martin Hempel[b], Serena Preyer[a]

[a] Department of Otolaryngology - Head and Neck Surgery, ViDia Christian Hospitals Karlsruhe, Germany
[b] Department of Neuroradiology, University Hospital Tübingen, Germany

2. Morphologic measurements of 3D Eustachian tube model and its prognostic value regarding Eustachian tube dysfunction

Authors
Savvas Kourtidis[a], Serena Preyer[a], Johann-Martin Hempel[b]

[a] Department of Otolaryngology - Head and Neck Surgery, ViDia Christian Hospitals Karlsruhe, Germany
[b] Department of Neuroradiology, University Hospital Tübingen, Germany

Savvas Kourtidis

Karlsruhe, den 20.01.2020

9. Acknowledgements

I would like to express my deepest gratitude to my tutor Prof. Serena Preyer for the continuous support throughout my clinical and academical education. She was my inspiration to pursue my doctoral degree.

The completion of my dissertation would not have been possible without the substantial contribution of Dr. med. Johann-Martin Hempel and Dr. Gunnar Blumenstock.

I would like to extend my sincere thanks to my family for the moral and emotional support in my life. They are helping me in all things, great and small.

Special thanks to Thanasis and Theodoros Ladas, both inspiring persons and good friends for lifetime.